



# Impact of morphological parameters on urban ventilation in compact cities: The case of the Tuscolano-Don Bosco district in Rome

Olga Palusci<sup>a,b,\*</sup>, Paolo Monti<sup>a</sup>, Carlo Cecere<sup>a</sup>, Hamid Montazeri<sup>b</sup>, Bert Blocken<sup>b,c</sup>

<sup>a</sup> Department of Civil, Building and Environmental Engineering, Faculty of Civil and Industrial Engineering, Sapienza University of Rome, Italy

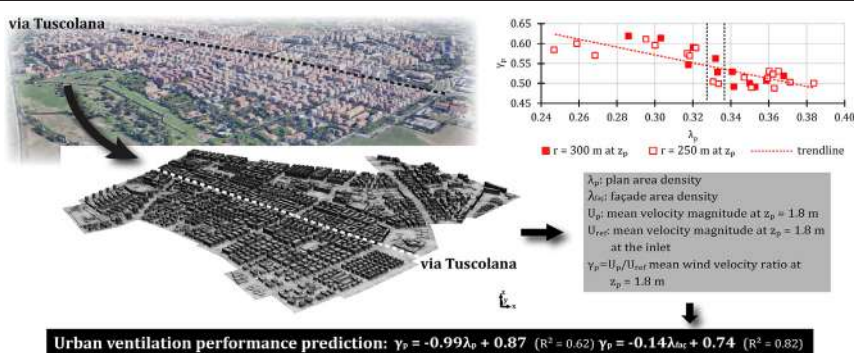
<sup>b</sup> Building Physics and Services, Department of the Built Environment, Eindhoven University of Technology, P.O. box 513, 5600 MB Eindhoven, the Netherlands

<sup>c</sup> Building Physics and Sustainable Design, Department of Civil Engineering, Leuven University, Kasteelpark Arenberg 40 – bus 2447, 3001 Leuven, Belgium

## HIGHLIGHTS

- Urban ventilation is assessed through CFD simulation for a large compact area in Rome.
- Linear models for predicting areas vulnerable to poor air conditions are provided.
- Reduction in the wind velocity up to 62% is experienced at the pedestrian level.
- Strong correlations between morphological parameters and urban ventilation are found.
- $\lambda_p = 0.33$  corresponds to a critical value for ventilation performance.

## GRAPHICAL ABSTRACT



## ARTICLE INFO

### Article history:

Received 19 April 2021

Received in revised form 6 September 2021

Accepted 17 September 2021

Available online 23 September 2021

Editor: Pavlos Kassomenos

### Keywords:

Urban ventilation  
Urban morphology  
Compact city  
CFD  
Mean velocity ratio  
Urban renovation plan

## ABSTRACT

Air pollution and heat stress are major concerns associated with the liveability, resilience and sustainability of cities. They directly affect health and comfort and are associated with augmented morbidity and mortality and an increase in the energy demand for building ventilation, air cleaning and cooling. Nevertheless, the detrimental effects of poor air quality may partly be mitigated by increased urban ventilation. This strategy is closely related to the level of urbanization and the urban morphology. Therefore, detailed investigations on the impact of different morphologies on urban ventilation are of paramount importance. Computational Fluid Dynamics simulations have been widely used during the last decades to investigate the effects of the urban morphology on the urban ventilation. However, most of these studies focused on idealized building arrangements, while detailed investigations about the role of real urban morphologies are scarce. This study investigates the ventilation in a compact area in the city of Rome, Italy. 3D steady-state Reynolds-averaged Navier-Stokes simulations are performed to analyze the impact of Morphological Parameters (MP) on the urban ventilation. The results show a considerable worsening of urban ventilation with increasing building density with a reduction in the mean wind velocity up to 62% experienced at the pedestrian level ( $z_p$ ). Correlations between five MPs, e.g., plan area density, area-weighted mean building height, volume density, façade area density, and non-dimensional mean velocity at pedestrian level and at 10 m height are evaluated, and simple models are obtained using linear regression analysis. Among the selected MPs, the building façade area density shows a remarkable correlation with the non-dimensional mean velocity at  $z_p$  ( $R^2 = 0.82$ ). Such correlations can be valuable tools for practitioners and urban designers, particularly during the first stage of planning, for highlighting areas potentially vulnerable to poor air conditions without running computationally expensive simulations.

© 2021 The Authors. Published by Elsevier B.V. This is an open access article under the CC BY license (<http://creativecommons.org/licenses/by/4.0/>).

\* Corresponding author at: Department of Civil, Building and Environmental Engineering, Faculty of Civil and Industrial Engineering, Sapienza University of Rome, Italy.  
E-mail address: [olga.palusci@uniroma1.it](mailto:olga.palusci@uniroma1.it) (O. Palusci).

**Nomenclature**

CFD	computational fluid dynamics
MP	morphological parameter
SDG	sustainable development goal
UC	urban canyon
AR	aspect ratio
$\lambda_p$	plan area density
$\lambda_f$	frontal area density
wVR	wind velocity ratio
WT	wind tunnel
U	mean wind speed
k	turbulence kinetic energy
$\varepsilon$	turbulence dissipation rate
q	hit rate
FAC2	factor of 2 of the observations
FAC1.3	factor of 1.3 of the observations
RE k- $\varepsilon$ model	realizable k- $\varepsilon$ model
STD k- $\varepsilon$ model	standard k- $\varepsilon$ model
RNG k- $\varepsilon$ model	Renormalization Group k- $\varepsilon$ model
H	building height
$H_m$	mean building height
$H_\sigma$	root mean square of the building heights
$H_{med}$	median of the building heights
$H_{aw}$	area-weighted mean building height
$\lambda_{vol}$	volume density
$\lambda_{fac}$	façade area density
$z_p$	pedestrian level height
$\gamma_p$	mean wind velocity ratio at $z_p = 1.8$ m
$\gamma_{10}$	mean wind velocity ratio at 10 m height
$U_{ref}$	mean velocity magnitude at reference height
$U_p$	mean velocity magnitude at 1.8 m
$U_{10}$	mean velocity magnitude at 10 m height
AI	area of interest

**1. Introduction**

Nowadays, more than 55% of the world population lives in urban areas (United Nations, 2018a) and this number keeps growing due to the increase in number, size and density of cities (United Nations, 2018b), which are enlarging their environmental footprint. Consequently, the challenge towards more sustainable and resilient built environments has become urgent, especially in existing cities. Many efforts are being made worldwide. In this regard, the adoption in 2015 by all United Nations Member States of the 2030 Agenda for Sustainable Development is significant. In the Agenda, seventeen Sustainable Development Goals (SDGs) have been identified to guarantee prosperity. The third and the eleventh goals explicitly state that it is necessary to “ensure healthy lives and promote well-being for all at all ages” and to “make cities and human settlements inclusive, safe, resilient and sustainable” (United Nations, 2015).

Currently, air pollution and heat stress are two major concerns (Oke and Maxwell, 1975; Neophytou and Britter, 2005; Ng, 2009; Hang et al., 2012a; Blocken, 2015; Toparlal et al., 2017) directly associated with the liveability, resilience and sustainability of cities. In Europe, more than 74% of the population lives in urban areas (United Nations, 2014), and over 90% of the urban population is exposed to air pollution (UNECE, 2018). Air pollution and heat stress have been linked to augmented morbidity and mortality (Seaton et al., 1995; Gasparrini et al., 2015; Cárdenas Rodríguez et al., 2016; WHO, 2016; Watts et al., 2018; Mitchell et al., 2019). However, the detrimental effects of air pollution and heat stress can – at least partly – be mitigated by increased urban ventilation (Ng, 2009). Urban ventilation represents the capacity of a built area for introducing fresh air within its tissues and diluting pollutants and heat within its canyons. This phenomenon is closely related to the level of urbanization and the urban morphology, i.e., the form and the structure of the

urban area, the physical characteristics of the buildings and their mutual arrangement. Conversely, urban morphology can be used as an effective tool in renovation plans for improving the urban ventilation.

For this purpose, two in-depth analyses are of paramount importance: detailed investigations of the impact of different morphologies on urban ventilation; and the identification of parameters and indicators that can describe the various characteristics of the urban morphology quantitatively. To be able to evaluate the impact of morphological parameters on the urban ventilation, investigations are generally conducted at the street scale, less than ~100 to 200 m, and at the neighborhood scale, up to 1 or 2 km, depending on the features of interest (Britter and Hanna, 2000). Given the complexity of the phenomenon, the majority of the studies performed in the past used simplified models of actual urban areas.

The simplified models are generic urban geometries selected based on the phenomenon under investigation. A review of morphological parameters used for generic urban geometries in urban ventilation studies is provided in Section 2.1. Albeit useful to investigate the contribution of specific parameters, these simplified models may not reproduce the complexity of the built environment. Exploring the relationship between urban ventilation and morphology has gained popularity in the literature in the past two decades; however, detailed investigations on the role of real urban morphologies are still required. Works conducted using actual urban areas as case studies are, in fact, very rare (Kubota et al., 2008; Yang et al., 2013; Tschritzis and Nikolopoulou, 2019). Section 2.2 provides a review of urban ventilation studies for actual urban areas along with methodology and morphological parameters. Other previous studies with numerical simulations in actual urban areas were performed; however, their aim was rarely to provide simplified models or guidelines generalizing the results. In fact, the simulations were usually conducted for: describing phenomena in specific case studies such as pollutant dispersion and reduction (Gousseau et al., 2011; Nozu and Tamura, 2012; Blocken et al., 2016; Jeanjean et al., 2017; Vervoort et al., 2019; Longo et al., 2020; Pelliccioni et al., 2020; Lauriks et al., 2021), and urban microclimate (Ashie and Kono, 2011; Toparlal et al., 2015; Toparlal et al., 2017; Antoniou et al., 2019; Conigliaro et al., 2021), or for verifying the accuracy of CFD (Antoniou et al., 2017; Ricci et al., 2017) and assessing the sensitivity of boundary conditions (An et al., 2013) and computational domains (Liu et al., 2018).

Given the lack of studies investigating the impact of real urban morphologies, this paper presents Computational Fluid Dynamics (CFD) simulations of the impact of the urban morphology on the ventilation within an area of the city of Rome, Italy, i.e., the Tuscolano-Don Bosco district. The urban morphology is described by a set of seven Morphological Parameters (hereinafter MPs) and their combinations, common among practitioners, policymakers and designers. This choice is motivated by the necessity of linking two specialist sectors: on the one hand, wind engineering and, on the other hand, building design and urban planning. The urban ventilation is expressed in terms of the mean wind speed ratio that in the past proved to be a useful indicator for this kind of analysis (Kubota et al., 2008; Yim et al., 2009; Hu and Yoshie, 2013; Yang et al., 2013; Ramponi et al., 2015; Du et al., 2017; Tschritzis and Nikolopoulou, 2019). An overview of indicators commonly employed in urban ventilation studies is provided in Section 2.3. Relations between each MP and the spatially averaged mean wind speed ratio at pedestrian level and 10-m height are discussed and correlations obtained using linear regression analysis are provided. CFD is used for this investigation because it allows full control over the boundary conditions and provides information on the flow within the entire domain without suffering from potential problems due to similarity requirements (Blocken, 2014; Di Bernardino et al., 2021).

**2. Literature review on morphological parameters and performance indicators**

This section reports a review of studies on urban ventilation highlighting: the morphological parameters used for generic

configuration (Section 2.1); the morphological parameters used for actual urban areas (Section 2.2); and the performance indicators (Section 2.3).

## 2.1. Literature review of morphological parameters for generic urban geometries

The simplified models are usually composed of generic building geometries forming idealized urban structures. They are usually represented by 2D and 3D urban canyons (UCs) and 3D urban arrays composed of aligned or staggered elements. The simplified model types are selected based on the features of the phenomenon at the local scale under investigation. An overview of morphological parameters used in urban ventilation studies for generic urban configurations is presented in Table 1. In studies performed using 2D UCs, the different urban morphologies are often parameterized using the so-called UC aspect ratio (H/W or height-to-width ratio), hereinafter referred to as AR (Sini et al., 1996; Xie et al., 2005a; Xie et al., 2005b; Xiaomin et al., 2006; Cheng et al., 2008; Ho et al., 2015; Badas et al., 2017; Di Bernardino et al., 2017; Di Bernardino et al., 2018), the roof shape (Xie et al., 2005b; Badas

et al., 2017) and the height or height variation (Xie et al., 2005a; Xie et al., 2005b; Xiaomin et al., 2006). Regarding the 3D UCs, besides the AR (Hunter et al., 1990; Hunter et al., 1992; Hang et al., 2010a; Hang et al., 2010b; Hang et al., 2012a; Ai and Mak, 2017); the roof shape (Llaguno-Munitxa and Bou-Zeid, 2018), the height or height variation (Hang et al., 2010a; Nardecchia et al., 2018); the L/W or UC length-to-width ratio (Hang et al., 2010a; Hang et al., 2012a), and the L/H or UC length-to-height ratio (Hunter et al., 1990; Hunter et al., 1992) are often considered in the parameterization. Moreover, the orientation of the UC compared to the direction of the approaching wind is another important parameter (Hang et al., 2010a). Finally, in studies using 3D urban arrays, the focus is on: AR (Hang et al., 2011; Hang and Li, 2011), L/H (Hang and Li, 2011), array layout types (Cheng and Castro, 2002; Coceal et al., 2006; Kanda, 2006; Hagishima et al., 2009; Hu and Yoshie, 2013), building footprint density expressed in terms of plan area density  $\lambda_p$  (i.e. the ratio between the total area of building footprints and the total land area) (Cheng and Castro, 2002; Kanda, 2006; Santiago et al., 2008; Hagishima et al., 2009; Buccolieri et al., 2010; Hang et al., 2011; Hang and Li, 2011; Hu and Yoshie, 2013; Razak et al., 2013; Cantelli et al., 2015; Chen et al., 2017; Di Bernardino et al., 2020a), building height or building height variation (Kanda, 2006; Hagishima et al., 2009; Yim et al., 2009; Hang and Li, 2011; Hang et al., 2012b; Razak et al., 2013; Lin et al., 2014; Hang et al., 2015; Chen et al., 2017), frontal area density  $\lambda_f$  (i.e. the ratio between the total projected area of building vertical surfaces facing the approaching wind direction and the total land area) (Cheng and Castro, 2002; Santiago et al., 2008; Hagishima et al., 2009; Razak et al., 2013; Chen et al., 2017; Ikegaya et al., 2017; Di Bernardino et al., 2020b), orientation (Soulhac et al., 2009; Yim et al., 2009; Amicarelli et al., 2012; Hang et al., 2013; Lin et al., 2014; Hang et al., 2015; Ramponi et al., 2015) and canopy roof covers (Hang et al., 2013).

## 2.2. Literature review of morphological parameters for actual urban areas

Despite the possibility of investigating specific parameters, the simplified models only partially represent the complexity of actual urban areas where different building typologies coexist within the urban tissues. A detailed investigation on the ventilation in actual urban areas is therefore necessary. To the best of the authors' knowledge, there are only a few studies that have investigated the effects of urban morphologies on wind conditions thoroughly using real case studies. Among the others, Kubota et al. (2008) carried out wind tunnel experiments for 22 cases representing actual residential neighborhoods in Japan. Yang et al. (2013) conducted field measurements in 10 residential sites in Shanghai, China and Tschrititz and Nikolopoulou (2019) performed numerical simulations for 24 cases taken from the Greater London area. Specifically, Kubota et al. (2008) studied the correlation between building density and spatially averaged wind velocity at the pedestrian level. The building density was expressed in terms of gross building cover ratio (equivalent to  $\lambda_p$ ) and gross floor area ratio (the ratio between the total area of building levels and the total land area). As for the ventilation, the wind velocity ratio, i.e., the ratio between the wind velocity measured at the height of interest, in this case the pedestrian level, and that at a reference height, was used for the assessment. Focusing separately on detached and apartment buildings, they found a strong correlation between  $\lambda_p$  and the wind velocity ratio for values of  $\lambda_p$  between 0.1 and 0.34. Yang et al. (2013), instead, analyzed the correlation between the pedestrian-level wind velocity ratio and the urban density, quantified by  $\lambda_p$ , the sky view factor, the tree view factor and the green plot ratio. They concluded that the pedestrian-level wind velocity ratio is significantly correlated with the density of the urban sites, highlighting the necessity to test their results under a more strictly controlled experimental environment. Finally, Tschrititz and Nikolopoulou (2019) analyzed the correlation between urban morphology and pedestrian wind comfort. They quantified the urban morphology

**Table 1**  
Overview of morphological parameters used in urban ventilation studies for generic urban configurations.

Idealized model types	Morphological parameters	Refs
2D urban canyons	Aspect ratio	Sini et al. (1996); Xie et al. (2005a); Xie et al. (2005b); Xiaomin et al. (2006); Cheng et al. (2008); Ho et al. (2015); Badas et al. (2017); Di Bernardino et al. (2017); Di Bernardino et al. (2018)
	Roof shape	Xie et al. (2005b); Badas et al. (2017)
	Building height or height variation	Xie et al. (2005a); Xie et al. (2005b); Xiaomin et al. (2006)
	Aspect ratio	Hunter et al. (1990); Hunter et al. (1992); Hang et al. (2010a); Hang et al. (2010b); Hang et al. (2012a); Ai and Mak (2017)
3D urban canyons	Roof shape	Llaguno-Munitxa and Bou-Zeid (2018)
	Building height or height variation	Hang et al. (2010a); Nardecchia et al. (2018)
	Length-to-width ratio	Hang et al. (2010a); Hang et al. (2012a)
	Length-to-height ratio	Hunter et al. (1990); Hunter et al. (1992)
	Orientation	Hang et al. (2010a)
	Aspect ratio	Hang et al. (2011); Hang and Li (2011)
	Length-to-height ratio	Hang and Li (2011)
	Array layout types	Cheng and Castro (2002); Coceal et al. (2006); Kanda (2006); Hagishima et al. (2009); Hu and Yoshie (2013)
3D urban arrays	Plan area density $\lambda_p$	Cheng and Castro (2002); Kanda (2006); Santiago et al. (2008); Hagishima et al. (2009); Buccolieri et al. (2010); Hang et al. (2011); Hang and Li (2011); Hu and Yoshie (2013); Razak et al. (2013); Cantelli et al. (2015); Chen et al. (2017); Di Bernardino et al. (2020a)
	Building height or height variation	Kanda (2006); Hagishima et al. (2009); Yim et al. (2009); Hang and Li (2011); Hang et al. (2012b); Razak et al. (2013); Lin et al. (2014); Hang et al. (2015); Chen et al. (2017)
	Frontal area density $\lambda_f$	Cheng and Castro (2002); Santiago et al. (2008); Hagishima et al. (2009); Razak et al. (2013); Chen et al. (2017); Ikegaya et al. (2017); Di Bernardino et al. (2020b)
	Orientation	Soulhac et al. (2009); Yim et al. (2009); Amicarelli et al. (2012); Hang et al. (2013); Lin et al. (2014); Hang et al. (2015); Ramponi et al. (2015)
	Canopy roof cover	Hang et al. (2013)



using four parameters: the mean building height, the maximum building height, the standard deviation of the building height and the façade area ratio. The pedestrian wind comfort was evaluated using wind comfort criteria performing numerical simulations for eight wind directions. Among the different morphological indicators, the façade area ratio has a dominant impact on the mean wind speed ratio and the percentage of outdoor space that is comfortable for certain activities.

### 2.3. Literature review of performance indicators in urban ventilation studies

In the last decade, the spatially averaged wind velocity ratio (wVR) has been proven as a useful indicator for evaluating urban ventilation. Among different purposes, it has been used for:

- investigating the relevance of different morphological parameters or building characteristics in aligned and staggered buildings arrays (Bady et al., 2011; Hu and Yoshie, 2013; Razak et al., 2013; Lin et al., 2014; Carpentieri and Robins, 2015; Sha et al., 2018);
- analyzing the pedestrian comfort related to low wind speed (Du et al., 2017);
- evaluating computational settings (Ai and Mak, 2017);
- supporting optimization procedures (Juan et al., 2017; Wen et al., 2017; Du et al., 2018; Du et al., 2019).

Besides spatially averaged wind velocity ratios, other indicators and methodologies have been employed for investigating the aerodynamic response of urban areas through:

- the description of the exchange between in-canopy and above-canopy flows (Bentham and Britter, 2003; Panagiotou et al., 2013; Chen et al., 2017);
- the analysis of pollutant concentration fields (Skote et al., 2005; Di Sabatino et al., 2007; Hang et al., 2009a, 2009b, 2009c; Hang et al., 2009a);
- the evaluation of drag and pressure coefficient (Lee and Soliman, 1977; Hussain and Lee, 1980; Kanda, 2006; Santiago et al., 2008; Hagishima et al., 2009; Buccolieri et al., 2017);

- the application of indices mainly developed for indoor ventilation studies (Sandberg, 1981) and eventually modified for outdoor investigations, e.g., air exchange rate, visitation frequency, residence time, purging flow rate, age of air, etc. (Peng et al., 2020; Huang et al., 2006; Cheng et al., 2008; Kato and Huang, 2009; Bady et al., 2008; Hang et al., 2009a; Bu et al., 2009; Hang and Li, 2010; Hang et al., 2011; Hang and Li, 2011; Hang et al., 2010a, 2010b; Hang et al., 2010b; Buccolieri et al., 2010; Hang et al., 2012a; Hang, Li, Sandberg, et al., 2012; Hang et al., 2013; Lin et al., 2014; Hang et al., 2015; Ramponi et al., 2015; Mei et al., 2017; Antoniou et al., 2017; Liu et al., 2017; Peng et al., 2019).

### 3. Description of the case study

To evaluate the impact of morphological parameters on the urban ventilation, a large compact area in Rome is selected, i.e., the Tuscolano-Don Bosco district. The Tuscolano-Don Bosco district is chosen as an example of a compact city in a Mediterranean climate. Details of the meteorological conditions typically observed in the Roman area can be found in Monti and Leuzzi (2005); Pelliccioni et al. (2015); Di Bernardino et al. (2021). This section introduces the characteristics of the Tuscolano-Don Bosco district, including information about the building typologies and urban morphologies present in the area, and describes the parameters used for the morphological analyses.

#### 3.1. Area of interest

The Tuscolano-Don Bosco district in Rome is chosen as a case study for investigating the impact of the urban morphology on ventilation. The Tuscolano-Don Bosco district can be considered representative of a compact city in the Mediterranean area in terms of its morphological and typological characteristics. The district is located in the South-East part of Rome (41°51'25.1" N 12°33'43.5" E), 6 km from the city center (identified with the Colosseum in Fig. 1a) and around 5 km from the Ciampino airport (Fig. 1a). Apart from an original nucleus dating back to the early 20th century, the neighborhood quickly developed in the

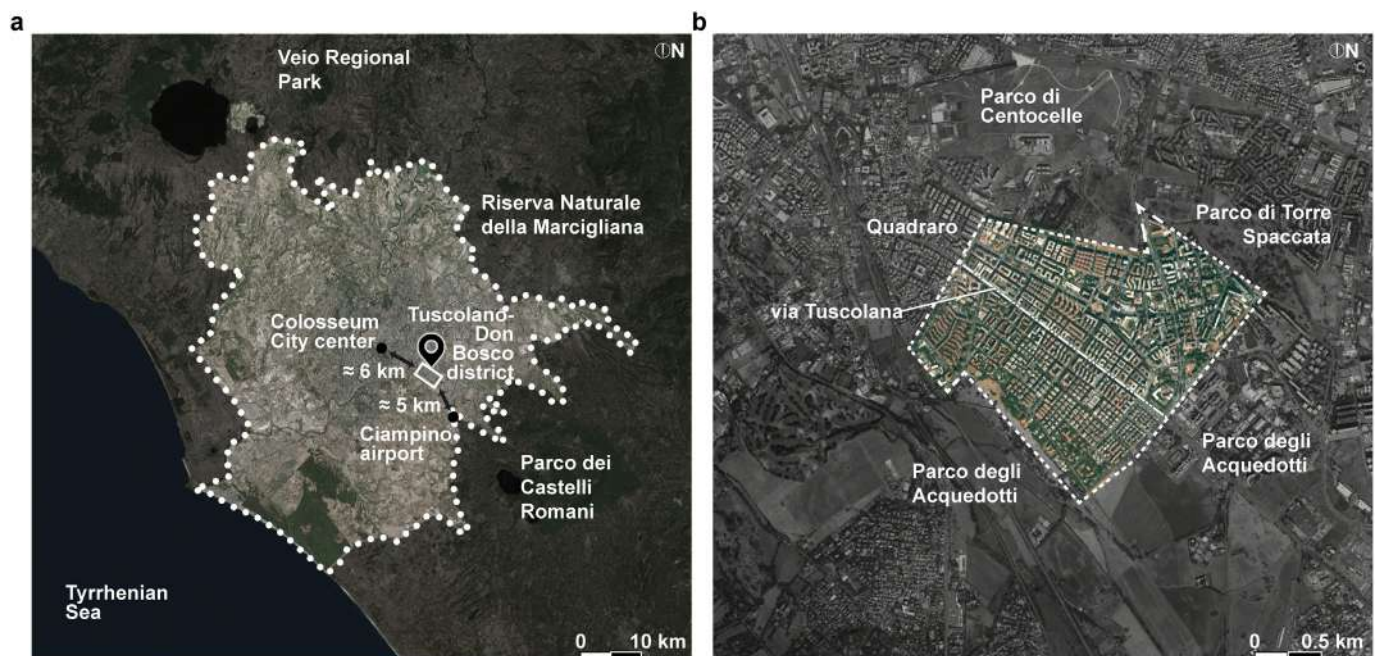


**Fig. 1.** (a) Map of Rome, including the Tuscolano-Don Bosco district location (white rectangle), (modified from Geoportale Italiano); and (b) detailed map with indication of the urban area modeled explicitly in the computational domain (white dotted line), (modified from Google Earth 2009).

aftermath of the World War II to respond to the urgent need for housing. Consequently, the district became one of the most densely populated in the city, with about 10,000 people per km<sup>2</sup> (*Ragioneria Generale I Direzione Sistemi informativi di pianificazione e controllo finanziario U.O. Statistica, 2017*), with an average  $\lambda_p$  above 0.3. The boundaries of the area of interest within the district are well defined (*Fig. 1b*): on the North by Centocelle park, on the North-East by Torre Spaccata park, on the East by the commercial-administrative pole of Cinecittà, on the South degli Acquadotti park, and on the West by the railway and the Quadraro neighborhood.

The district developed according to an orthogonal grid along the main street, via Tuscolana, which represents the backbone of the entire district (*Figs. 1b–2*). The longitudinal axis of this street is oriented at an angle of 40° to the South. Therefore, it is possible to identify two sub-areas: one on the North and the other on the South of via Tuscolana. The former is characterized by higher buildings, larger public spaces (squares and boulevards) and longer UCs compared to the latter (*Fig. 2a*). Moreover, the urban morphologies in the northern area are more compact with a predominance of towers and courtyards. Furthermore, the presence of podiums hosting commercial activities occupying the first 4–8 m of the buildings is very common in this area. The morphologies belonging to the southern area, instead, can be referred to as open with a prevalence of multi-story slabs, pavilions and “palazzina”, a characteristic building typology of Rome similar to the pavilion but with fewer stories. Overall, the district is mainly composed of narrow streets with  $0.7 < AR \leq 2.5$ . The building height varies significantly according to the different typologies within the district; the mean height is above 20 m, while its maximum is about 40 m. A scarce presence of vegetation is registered. All the above-mentioned morphological characteristics are typical of the so-called Mediterranean compact city (*Salvati et al., 2019*).

In order to conduct a detailed and systematic investigation, it has been decided to analyze the airflow in portions of the area of interest, hereinafter called areas of investigation (AIs). The constraints imposed for the selection of the AIs are (i) circular shape; (ii) the presence of at least one row of buildings around the AI for every wind direction analyzed (*Yoshie et al., 2007; Tominaga et al., 2008*); (iii) a sufficient number of cases “randomly” chosen, from a morphological point of view, i.e., the AIs should present inhomogeneous morphologies.

Since very long urban canyons (above 200 m long) are present in the northern sub-area, it has been decided to work with AIs of 300 m (total number of AIs equal to 12) and 250 m radius (total number of AIs equal to 19) in order to avoid that the urban canyon length will interfere significantly with the results. The centers of the AIs are aligned on orthogonal grids (one for 250 m and one for 300 m radius AIs) and generally placed every 200 m both longitudinally and transversally. *Fig. 2* shows a grey-scale map of building heights, including the locations of every AI center: red cross for 250 m radius AIs and iced blue for 300 m radius AIs.

### 3.2. Urban morphological parameters

The calculation of the MPs describing real cities is a nontrivial task because of the complexity of the urban textures (*Grimmond and Oke, 1999; Ratti et al., 2006; Berghauser Pont and Haupt, 2009; Salvadori et al., 2021*). Since this study aims at assessing the impact of the urban morphology on the ventilation within a real compact urban area, the first step of the investigation is the identification of MPs, and their combinations, able to describe the different morphologies and quantify the building density and the vertical structures of cities. Among the MPs generally employed in urban canopy studies, it is chosen not to use directional parameters because this study aims to provide a prediction model to be used in the early stage of

the design. Therefore, MPs used by practitioners and urban planners, which are usually non-directional, seem to be the best choice. Specifically, the MPs used in this study are: plan area density  $\lambda_p$ , mean building height ( $H_m$ ), root mean square of the building heights ( $H_{\sigma}$ ), median of the building heights ( $H_{med}$ ), area-weighted mean building height ( $H_{aw}$ ), volume density ( $\lambda_{vol}$ ), i.e., ratio between total building volume and total land surface, and façade area density ( $\lambda_{fac}$ ), i.e., ratio between total building vertical surfaces and total land area. *Fig. 3* presents the building characteristics of interest and some of the MPs used in the present study. Note that the façade area density  $\lambda_{fac}$  is different from the frontal area density  $\lambda_f$  because the former is the ratio between the building façade area and the land area, while the latter is the ratio between the projected area of building façades facing the wind and the land area.  $H_{aw}$  has been introduced as a possible alternative to more consolidated parameters such as  $H_m$ ,  $H_{\sigma}$ , and  $H_{med}$  to take the presence of the podiums that characterize the area of interest better into account.

The morphological analyses have been carried out using two versions of the open-source GIS software QGIS (*QGIS Documentation, 2021*), namely v. 2.14 and 3.2.3. The primary data are the open data provided by the regional authority (*Carta Tecnica Regionale, 2016*) and consist of information about the footprint area and the elevation above sea level of the foot and the top of every building. The quality of the raw data has been checked for the entire modeled area, and, when necessary, field surveys have been conducted. The raw data have been processed to extract information about land area, building footprint area, and building height. Then, several algorithms and scripts have been used to combine the basic information in order to calculate the selected morphological parameters. *Table 2* reports the values of the 7 MPs calculated for the 31 AIs. Note that  $\lambda_p$  ranges between 0.25–0.38, which is suggested by Oke as a suitable range to exclude the worst effects in terms of not providing shelter and not facilitating pollutant dispersion inside UCs (*Oke, 1988*). It is possible to divide the AIs into three groups based on the position of their centers in relation to via Tuscolana, i.e., N = North, S = South, T = on via Tuscolana. The presence of via Tuscolana and larger squares and boulevards in the northern area is evident by analyzing the  $\lambda_p$  for each group. The average values of  $\lambda_p$  are 0.32 for the N-group, 0.35 for the S-group, and 0.34 for the T-group; the maximum values are 0.37, 0.38, and 0.37, respectively; while the minimum values are 0.25, 0.32, and 0.26, respectively. Regarding  $H_m$ , the average values are 17.8 for the N-group, 18.7 for the S-group, and 18.3 for the T-group. Therefore, the S-group presents the highest value. Conversely, considering the average values of  $H_{aw}$ , the T-group shows the highest value. In fact, the average values are 22.5 for the N-group, 22.2 for the S-group, and 23.5 for the T-group. The discrepancy between  $H_m$  and  $H_{aw}$  may be due to podiums hosting commercial activities along via Tuscolana and in the northern area. This feature may also be confirmed by analyzing  $H_{\sigma}$ , the average values of which are 10.2 for the N-group, 8.3 for the S-group, and 9.8 for the T-group.

*Fig. 4a* shows the relations  $\lambda_p$ – $\lambda_{vol}$  and  $\lambda_p$ – $\lambda_{fac}$ , which highlight interesting characteristics of the building typologies of the Tuscolano-Don Bosco district. The two relations exhibit a strong correlation and monotonically increasing trends. The strong correlations and the absence of outliers are a consequence of the building characteristics as dictated by the different typologies present in the AIs, which are typical of the Mediterranean compact city. The increasing trends are the signature of the absence of typologies like skyscrapers or malls, which would result in low values of  $\lambda_p$  for large values of  $\lambda_{vol}$  and  $\lambda_{fac}$  or large values of  $\lambda_p$  for low values of  $\lambda_{vol}$  and  $\lambda_{fac}$ , respectively. These typologies, present in many contemporary cities, are not typical of the Mediterranean compact city. Therefore, it is possible to conclude that the chosen MP relationships can quantitatively and qualitatively describe the different morphologies present in the area of interest. Specifically,





**Fig. 2.** (a) Map of the height [m] of the buildings modeled in the domain with the locations of the center of the AIs; plan view of the 31 AIs considered in the study with (b) 300 m radius and (c) 250 m radius.

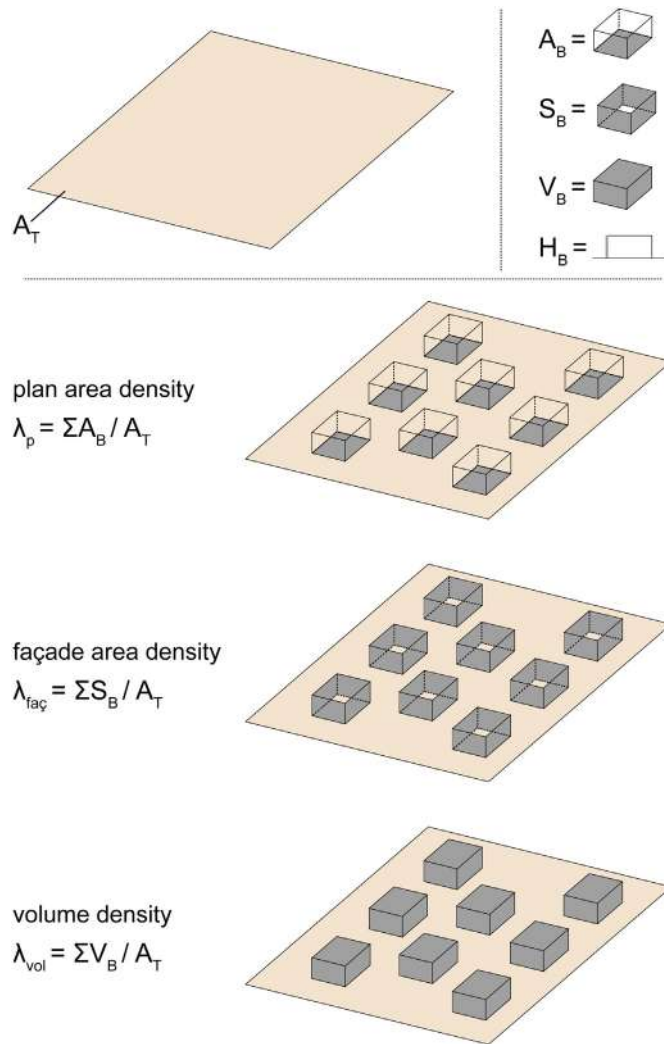


**Fig. 3.** Building characteristics and main morphological parameters used for characterizing the urban area:  $A_T$ : total area,  $A_B$ : building footprint area,  $S_B$ : building façade area,  $V_B$ : building volume, and  $H_B$ : building height.

they not only report quantities about the building density, volume and façade but can also provide insights into the building typologies present in the area as they correlate information regarding three densities, i.e., plan area density,  $\lambda_p$ , volume density,  $\lambda_{vol}$ , and façade area density,  $\lambda_{faç}$ . Another important characteristic to consider is the building height. This characteristic, if quantified using a set of indices like in this case, can provide information about the characteristics of the area, as explained above. However, unlike building volume and building façade, the building height is usually regulated by codes, and therefore correlations with the plan area density may be low, like in this case (Fig. 4b).

#### 4. CFD simulations

The present study investigates the ventilation in a large compact area in Rome, the Tuscolano-Don Bosco district, performing 3D steady-state Reynolds-averaged Navier-Stokes simulations. This section presents details about the computational domain and grid, the imposed boundary conditions and the chosen solver settings.

##### 4.1. Computational geometry and grid

The computational domain is built according to the best practice guidelines (Franke et al., 2007; Blocken et al., 2007; Tominaga et al.

**Table 2**

List of the morphological parameters calculated for each AI: radius of the AI ( $r$ ), position of the AI center in relation to via Tuscolana (N = North, S = South, T = on via Tuscolana), number of buildings ( $\#_B$ ), plan area density ( $\lambda_p$ ), mean building height ( $H_m$ ), root mean square of the building heights ( $H_o$ ), the median of the building heights ( $H_{med}$ ), area-weighted mean building height ( $H_{aw}$ ), volume density ( $\lambda_{vol}$ ), and façade area density ( $\lambda_{faç}$ ).

Als	r [m]	Center	# <sub>B</sub>	$\lambda_p$	$H_m$	$H_o$	$H_{med}$	$H_{aw}$	$\lambda_{vol}$	$\lambda_{faç}$
A <sub>1</sub>	300	N	149	0.34	15.87	10.33	18.00	23.27	7.93	1.49
B <sub>1</sub>	300	N	159	0.35	17.16	11.21	21.00	24.66	8.63	1.63
C <sub>1</sub>	300	N	146	0.33	17.70	11.62	21.00	25.10	8.36	1.54
D <sub>1</sub>	300	N	133	0.33	18.59	10.90	21.00	23.07	7.66	1.41
E <sub>1</sub>	300	N	131	0.32	17.21	10.44	21.00	22.03	7.05	1.29
F <sub>1</sub>	300	N	104	0.30	17.72	11.66	18.00	21.23	6.43	1.17
G <sub>1</sub>	300	N	95	0.29	18.49	9.16	21.00	19.59	5.61	1.02
H <sub>1</sub>	300	S	180	0.32	18.80	8.01	21.00	21.28	6.76	1.44
I <sub>1</sub>	300	S	223	0.34	19.10	8.69	21.00	23.91	8.17	1.78
J <sub>1</sub>	300	T	218	0.35	19.20	9.69	21.00	24.82	8.76	1.80
K <sub>1</sub>	300	T	188	0.37	18.20	10.80	21.00	24.38	8.97	1.69
L <sub>1</sub>	300	S	241	0.36	18.44	9.48	21.00	23.53	8.44	1.70
A <sub>2</sub>	250	N	106	0.37	14.92	10.87	10.00	23.24	8.49	1.55
B <sub>2</sub>	250	N	117	0.35	15.76	11.31	10.00	24.58	8.62	1.65
C <sub>2</sub>	250	N	93	0.33	17.87	12.07	24.00	25.55	8.45	1.56
D <sub>2</sub>	250	N	80	0.32	18.56	11.13	21.00	25.07	7.95	1.44
E <sub>2</sub>	250	N	79	0.32	16.73	9.78	18.00	21.07	6.78	1.24
F <sub>2</sub>	250	N	76	0.30	18.04	9.52	24.00	22.71	6.82	1.25
G <sub>2</sub>	250	N	68	0.30	17.07	9.87	16.50	17.09	5.05	0.91
H <sub>2</sub>	250	N	80	0.27	17.99	7.89	21.00	16.73	4.49	0.93
I <sub>2</sub>	250	N	79	0.25	21.00	8.41	24.00	19.87	4.91	1.01
J <sub>2</sub>	250	S	109	0.32	18.25	8.08	21.00	20.60	6.56	1.30
K <sub>2</sub>	250	N	148	0.33	19.17	8.56	21.00	23.90	7.97	1.71
L <sub>2</sub>	250	N	142	0.36	20.81	9.46	24.00	25.47	9.25	1.85
M <sub>2</sub>	250	T	148	0.37	18.20	11.04	21.00	24.86	9.23	1.83
N <sub>2</sub>	250	T	124	0.36	16.98	10.92	21.00	24.01	8.65	1.62
O <sub>2</sub>	250	T	114	0.26	18.80	6.52	21.00	19.53	5.06	1.12
P <sub>2</sub>	250	S	201	0.35	18.85	8.15	21.00	22.82	7.92	1.78
Q <sub>2</sub>	250	S	183	0.36	18.62	9.46	21.00	23.55	8.46	1.72
R <sub>2</sub>	250	S	162	0.38	18.95	9.24	21.00	22.11	8.48	1.64
S <sub>2</sub>	250	S	170	0.36	18.69	5.54	19.50	19.70	7.14	1.38

(2008); Blocken, 2015). Consequently, the height of the domain is equal to  $6H_{max}$ , where  $H_{max} = 40$  m is the height of the tallest building in the area. Furthermore, special care is given to allow the full development of the wake region irrespective of the wind direction. Therefore, the plan area of the computational domain is  $5000 \text{ m} \times 5000 \text{ m}$ , while the height is  $240 \text{ m}$  (Fig. 5a).

Over 1500 buildings belonging to the area of interest are modeled explicitly. The computational grid is generated using the surface-grid extrusion technique presented by van Hooff and Blocken (2010) that allows a large control of the grid quality. The grid consists of only hexahedral cells to avoid possible convergence problems associated with steady RANS simulations when second-order discretization schemes are used (Blocken, 2015). The non-conformal grid technique with a 1:2 ratio (Iousef et al., 2017) is applied in order to provide a detailed representation of the buildings and to limit the number of grid cells. Consequently, the domain is divided into three parts (Fig. 5b), where the core, region A, represents the area of interest. Here, the buildings are modeled explicitly, i.e., with their actual shape and size, with high resolution down to details of  $0.5 \text{ m}$  (Fig. 5b), while small façade and roof details are not included. Moreover, other urban elements, such as sidewalks, gardens, barriers, etc., are modeled implicitly by means of the corresponding values of the aerodynamic roughness length,  $z_0$  (Wieringa, 1992) converted to equivalent sandgrain roughness height  $k_s$  (Blocken et al., 2007). In regions B and C the grid is coarser but the growth ratio remains below 1.3 as recommended by the guidelines, e.g., Franke et al. (2007); Tominaga et al. (2008). All the urban elements, buildings included, are modeled implicitly using  $z_0$ .

In accordance with the recommendations by Franke et al. (2007) and Tominaga et al. (2008) regarding the evaluation of the pedestrian



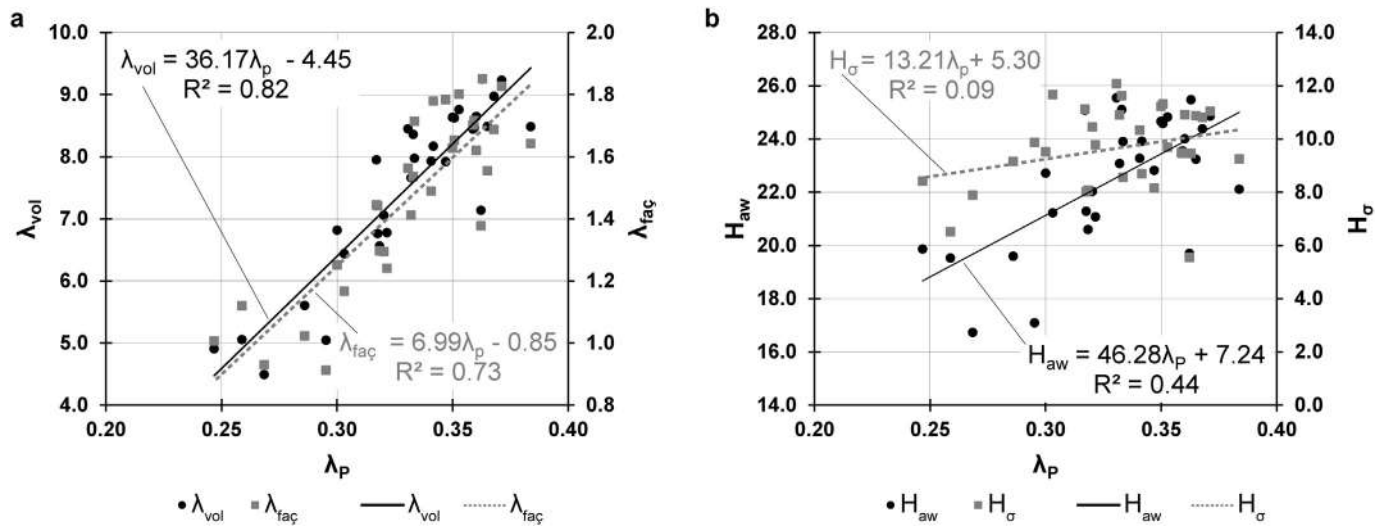


**Fig. 4.** (a) Volume density ( $\lambda_{vol}$ , black circles) and façade area density ( $\lambda_{faç}$ , grey squares) as a function of plan area density ( $\lambda_p$ ); (b) area-weighted mean building height ( $H_{aw}$ , black circles) and root mean square of the building height ( $H_{\sigma}$ , grey squares) as a function of plan area density ( $\lambda_p$ ).

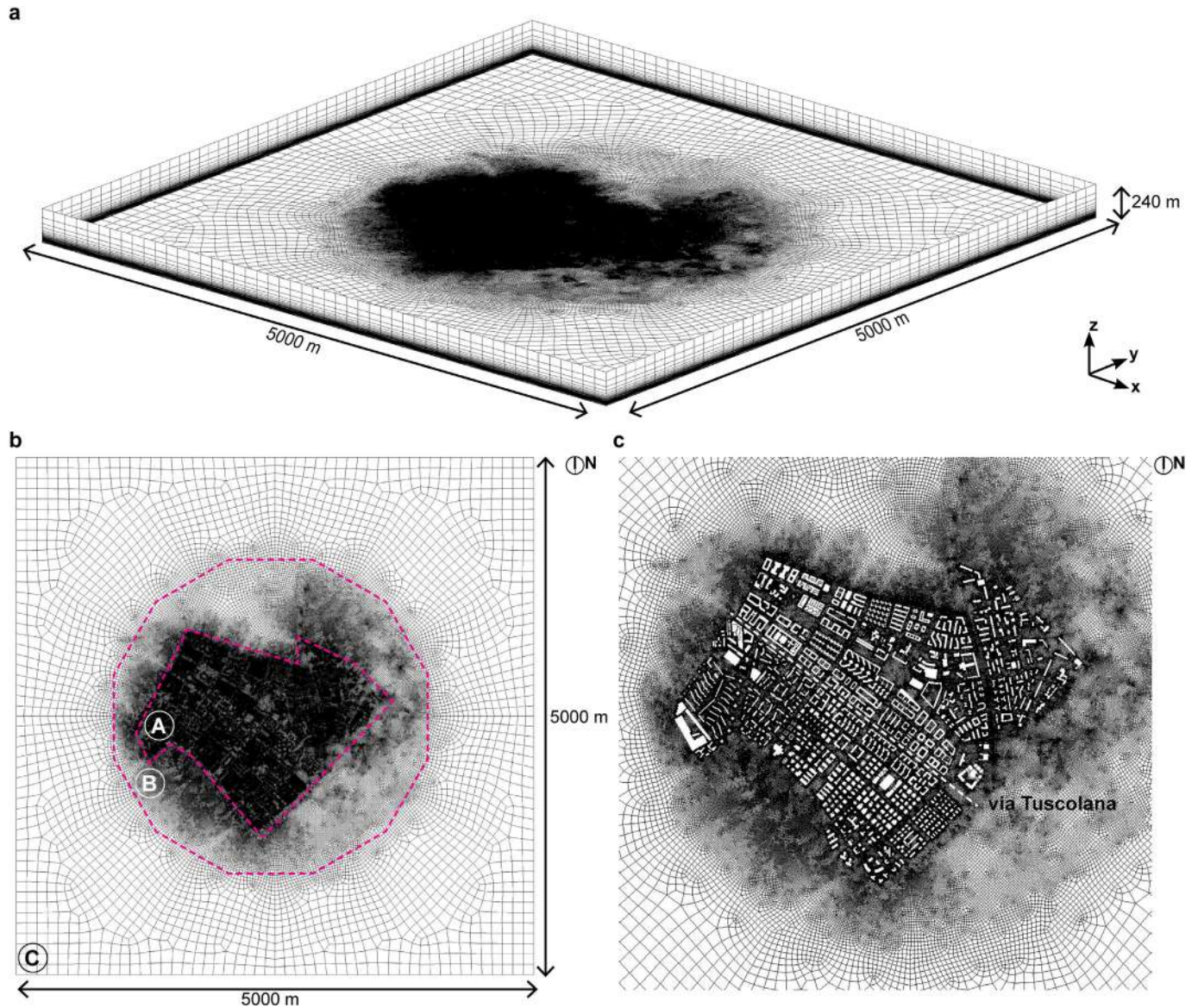


**Fig. 5.** (a) Axonometric view of the computational grid; (b) top view of the computational grid with non-conformal interfaces highlighted; (c) top view of the area of interest at 3 m height. Total cell count is about 86 million.



wind environment, the pedestrian level (1.8 m) is above the third cell layer. The resulting grid consists of about 86 million hexahedral cells (Figs. 5, 6). Note that a separate grid independence analysis for the case study grid is not performed, but that instead, in line with the vast majority of CFD studies for large urban areas (e.g., Oguro et al., 2008; Ashie and Kono, 2011; Tominaga, 2012; Gromke et al., 2015; Toparlar et al., 2015; Blocken et al., 2016; Antoniou et al., 2017; Montazeri et al., 2017; Ricci et al., 2017; Gao et al., 2018; Liu et al., 2018; Toparlar et al., 2018; Antoniou et al., 2019; Vervoort et al., 2019) and in agreement with the published best practice guidelines for such simulations, the grid resolution and grid topology of the case study are based on:

- General best practice guidelines for grid generation (Casey and Wintergerste, 2000; Tucker and Mosquera, 2001), such as those on cell orthogonality and wall-adjacent cell faces that should be either perpendicular or parallel to the adjacent wall;
- Specific best practice guidelines for studies on wind flow around buildings (Franke et al., 2007; Tominaga et al., 2008; Blocken, 2015), such as the minimum grid resolution of 10 cells along every building edge and across every passage between adjacent buildings;
- The grid resolution as resulting from the sub-configuration study (see Appendix A), where a grid independence analysis was performed.

#### 4.2. Boundary conditions

Since the simulations refer to neutral atmospheric conditions, the classical logarithmic law (e.g., Richards and Hoxey, 1993) for the vertical profile of the wind velocity,  $U$ , is used at the inlet:

$$U(z) = \frac{u_*}{\kappa} \ln \left( \frac{z + z_0}{z_0} \right) \quad (1)$$

while Eqs. (3) and (4) are employed to set  $k$  and  $\epsilon$ , respectively. The simulations are performed for 12 wind directions, equally spaced every 30°, starting from North (0°). A wind speed of 3 m/s at 10 m height is imposed at the inlet. The aerodynamic roughness length  $z_0$  is estimated based on the Davenport-Wieringa roughness classification (Wieringa, 1992) for each wind direction according to the land use map (Urban Atlas 2006, 2014). Three different values of  $z_0$  are used to model the urban area upwind of the domain: 0.25 m, 0.5 m, and 1.0 m. At the top of the domain, a symmetry boundary condition is applied, while zero static gauge pressure or symmetry boundary conditions are imposed at the domain sides, depending on the wind direction. For the bottom of the domain and the building surfaces, the standard wall functions by Launder and Spalding (1974) with roughness modification by Cebeci and Bradshaw (1977) are used. Specifically, four different classes are considered to model the urban surface: open ( $z_0 = 0.03$  m), rough ( $z_0 = 0.25$  m), very rough ( $z_0 = 0.50$  m), and closed ( $z_0 = 1.00$  m). The corresponding values of the roughness parameters, i.e., the sand-grain roughness height  $k_s$  (m) and the roughness constant  $C_s$ , are determined using their consistency relationship with the aerodynamic roughness length  $z_0$  derived by Blocken et al. (2007):

$$k_s = \frac{9.793 \times z_0}{C_s} \quad (2)$$

Smooth wall conditions are imposed at the building surfaces ( $k_s = 0$  and  $C_s = 0.5$ ).

#### 4.3. Solver settings

The same solver settings as in the validation study are applied. The validation study is reported in Appendix A. The 3D steady

RANS equations are solved in combination with the realizable k- $\epsilon$  model (Shih et al., 1995) using Ansys Fluent 16.2 (ANSYS FLUENT 15.0, 2013). For pressure-velocity coupling, the SIMPLE algorithm is used and second-order discretization schemes are applied. Finally, every simulation is run for 12,000 iterations and is terminated when the scaled residuals do not show any further reduction with an increasing number of iterations. The following minimum values are reached:  $10^{-5}$  for continuity and  $\epsilon$ ,  $10^{-4}$  for  $k$ ,  $10^{-7}$  for  $x$ -,  $y$ - and  $z$ -velocity.

## 5. Results and discussion

This section analyzes the relationships between the spatially averaged mean wind velocity ratio and the urban MPs considering the 12 wind fields simulated as described in Section 4.2. Two non-dimensional mean wind velocity ratios are used for the analysis, i.e.,  $\gamma_P = U_P/U_{ref}$  and  $\gamma_{10} = U_{10}/U_{ref}$ . Here,  $U_P$  and  $U_{10}$  are the values at pedestrian level ( $z_P = 1.8$  m) and at half of the average UC height ( $z_{10} = 10$  m), respectively, while  $U_{ref}$  is the mean velocity magnitude set at  $z_P$  at the inlet plane. Both ratios, which quantify the reduction in wind velocity caused by the urban canopy, are spatially averaged over each of the 31 AIs and then averaged over the 12 simulations (one for each wind direction imposed at the inlet). As mentioned earlier, this choice is due to the fact that MPs used by practitioners and urban planners are not directional. Furthermore, the averaging procedure should minimize unwanted effects associated with the directional (and therefore local) characteristics of the AIs.

Note that the non-dimensional wind velocity, when employed for investigating the relationship between urban morphology and urban ventilation in idealized urban textures, is usually estimated considering only one building typology. However, using a simplifying assumption such as idealized urban textures with only one building typology may not be acceptable in actual urban areas like the one considered in the present analysis, where the 31 AIs show different morphological characteristics.

#### 5.1. Model comparison with Kubota et al.'s experiments

Initially, some of the results are compared with those by Kubota et al. (2008), who conducted a series of experiments in the wind tunnel at the Niigata Institute of Technology for 22 case studies representing  $270 \times 270$  m<sup>2</sup> actual urban areas referring to major Japanese cities. The wind velocity was measured at approximately 50 points placed uniformly around the buildings in each area. Fig. 7 shows  $\gamma_P$  as a function of  $\lambda_P$  for all the 31 AIs in the present study (red solid squares: 300-m radius; red open squares: 250-m radius) and for the apartment-house types from Kubota et al. (black crosses). The first characteristic to highlight is that  $\gamma_P$  decreases monotonically with  $\lambda_P$ , i.e. there is an overall decrease in mean velocity for larger building densities. The  $\gamma_P$  trend emerging from the present CFD study is in good agreement with that found by Kubota et al. (2008) even though the data show a less strong correlation probably due to higher level of inhomogeneity of the urban morphology in the present study, as indicated by the coefficient of determination ( $R^2$ ). This agreement supports the CFD results and the methodology adopted in this work. Note that 250-m and 300-m cases exhibit a similar behavior. This suggests that the  $\lambda_P$ - $\gamma_P$  relationship is independent of the AI radius used for its determination.

#### 5.2. Impact of morphological parameters on $\gamma_P$ and $\gamma_{10}$

The urban ventilation is explored by analyzing  $\gamma_P$  and  $\gamma_{10}$ , computed for 300-m and 250-m radii, as a function of  $\lambda_P$ ,  $H_{aw}$ ,  $\lambda_{vol}$ ,  $\lambda_{fac}$ , and  $\lambda_{fac}/\lambda_P$ . Fig. 8 shows the relationships between each MP and  $\gamma_P$  and  $\gamma_{10}$ . For each MP- $\gamma_P$  and MP- $\gamma_{10}$  relation a simple model obtained using linear





**Fig. 6.** Perspective view of: (a) the area of interest (modified from Google Maps); (b) the computational grid and (c) its enlargement. Total cell count is about 86 million.



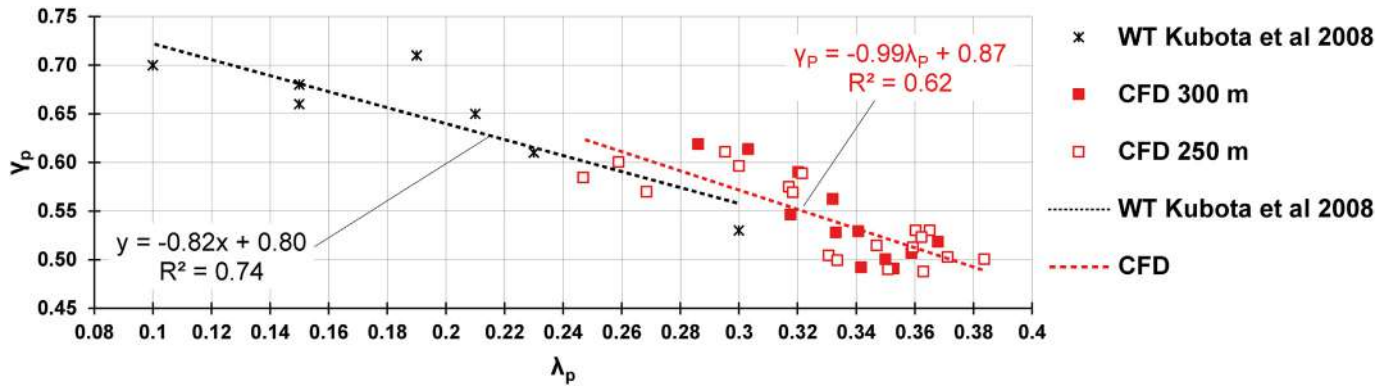


Fig. 7.  $\gamma_p$  versus  $\lambda_p$ . Solid and open red squares refer to  $\gamma_p$  obtained for the 31 AIs using the CFD data, while crosses denote  $\gamma_p$  based on wind-tunnel experiments by Kubota et al. (2008).

regression analysis is derived, indicating the correlation between the two variables by means of  $R^2$ .

Fig. 8a compares  $\gamma_p$  and  $\gamma_{10}$  as a function of  $\lambda_p$ .  $\gamma_p$  decreases monotonically with increasing  $\lambda_p$ , ranging from 0.62 to 0.49 with 0.54 as a mean value. This suggests that pedestrians experience, on average, a mean wind speed reduced by a factor of 0.54 with respect to the undisturbed velocity outside the city. On the other hand,  $\gamma_{10}$  falls in the 0.50–0.80 range with a 0.60 as a mean value and a larger deviation, above 37%. However, for  $\lambda_p > 0.33$  the two wind speed ratios tend to converge, i.e.,  $U_p \sim U_{10}$  for denser urban tissues and narrower canyons. Another salient feature is the abrupt reduction in  $\gamma_p$  and  $\gamma_{10}$  observed for  $\lambda_p = 0.33$ , where the latter seems to represent a sort of threshold value. In fact,  $\lambda_p$  no longer plays a significant role for  $\lambda_p > 0.33$  (at least for the considered  $\lambda_p$  range). Note that for  $\lambda_p < 0.33$  the data points are mainly placed above the trend line, while the opposite happens for  $\lambda_p > 0.33$ . This characteristic will be discussed further in the next subsection. The models derived for  $\lambda_p$ - $\gamma_p$  and  $\lambda_p$ - $\gamma_{10}$  are:

$$\gamma_p = -0.99\lambda_p + 0.87 \quad (3)$$

$$\gamma_{10} = -1.99\lambda_p + 1.26 \quad (4)$$

with  $R^2 = 0.62$  and  $R^2 = 0.63$ , respectively. As already found by Kubota et al. (2008), there is a strong linear relationship between  $\lambda_p$  and  $\gamma_p$ . The results reported in the present work show that a strong linear relationship also exists between  $\lambda_p$  and  $\gamma_{10}$ .

The impact of the building height variation on urban ventilation is assessed using  $H_m$ ,  $H_o$ ,  $H_{med}$ , and  $H_{aw}$ . Among these four MPs, the latter shows the strongest correlation with both  $\gamma_p$  and  $\gamma_{10}$ . For this reason, only the results related to  $H_{aw}$  are displayed in Fig. 8b, while the results related to  $H_m$ ,  $H_o$ ,  $H_{med}$  can be found in Appendix B. However, among the five key MPs in this section,  $\lambda_p$ ,  $H_{aw}$ ,  $\lambda_{vol}$ ,  $\lambda_{fac}$ , and  $\lambda_{fac}/\lambda_p$ ,  $H_{aw}$  is the one that shows the weakest correlation, especially at the pedestrian level ( $R^2 = 0.48$ ). Therefore, it has been decided not to report the models shown in Fig. 8b.

The dependence of the reduction in mean wind velocity ratio is apparent also for increasing  $\lambda_{vol}$  for both the pedestrian level and the 10-m height (Fig. 8c).  $\gamma_p$  decreases as the volume density increases and, for large values of  $\lambda_{vol}$ ,  $\gamma_p$  and  $\gamma_{10}$  tend to converge onto 0.5. The models derived for  $\lambda_{vol}$ - $\gamma_p$  and  $\lambda_{vol}$ - $\gamma_{10}$  are:

$$\gamma_p = -0.03\lambda_{vol} + 0.74 \quad (5)$$

$$\gamma_{10} = -0.05\lambda_{vol} + 1.01 \quad (6)$$

with  $R^2 = 0.68$  and  $R^2 = 0.75$ , respectively.

Fig. 8d reports the values of  $\gamma_p$  and  $\gamma_{10}$  as a function of  $\lambda_{fac}$ . A remarkable correlation for both  $\lambda_{fac}$ - $\gamma_p$  and  $\lambda_{fac}$ - $\gamma_{10}$  relations is

observed. The two trends decrease monotonically as  $\lambda_{fac}$  increases and converge onto 0.50 for  $\lambda_{fac} \sim 1.8$ .  $R^2$  is 0.82 and 0.89 for  $\gamma_p$  and  $\gamma_{10}$ , respectively. The fact that the best correlation occurs for  $\lambda_{fac}$  may be explained considering the nature of this parameter, which carries information on both the building height and the perimeter of the building footprint. This finding is in line with the results of previous studies (Tsichritzis and Nikolopoulou, 2019) and corroborates the methodology adopted in this work. The models derived for  $\lambda_{fac}$ - $\gamma_p$  and  $\lambda_{fac}$ - $\gamma_{10}$  are:

$$\gamma_p = -0.14\lambda_{fac} + 0.74 \quad (7)$$

$$\gamma_{10} = -0.29\lambda_{fac} + 1.03 \quad (8)$$

Finally, Fig. 8e shows the dependency of  $\gamma_p$  and  $\gamma_{10}$  on  $\lambda_{fac}/\lambda_p$ . The corresponding models are:

$$\gamma_p = -0.06 \frac{\lambda_{fac}}{\lambda_p} + 0.82 \quad (9)$$

$$\gamma_{10} = -0.14 \frac{\lambda_{fac}}{\lambda_p} + 1.23 \quad (10)$$

and present a significant correlation being  $R^2 = 0.63$  and  $R^2 = 0.76$ , respectively.

Overall, four main general observations are made:

- $\gamma_p$  and  $\gamma_{10}$  clearly depend on all five morphological parameters.
- $\gamma_p$  and  $\gamma_{10}$  do not depend on the AI radius.
- $\gamma_p$  and  $\gamma_{10}$  decrease monotonically with increases in the morphological parameters.
- $\gamma_p$  and  $\gamma_{10}$  tend to share the same value for denser urban tissues, suggesting that the impact of the height on the velocity ratio inside the canyon vanishes.

### 5.3. Further discussion

Focusing only on the impact of  $\lambda_p$  on  $\gamma_p$  and  $\gamma_{10}$ , three different behaviors in this relation can be distinguished (Fig. 9). A first plateau can be identified around  $\gamma_p = 0.6$  at pedestrian level ( $\gamma_{10} = 0.73$  at  $z = 10$  m) for  $\lambda_p \leq 0.31$ , while a second plateau with  $\gamma_p = 0.52$  ( $\gamma_{10} = 0.54$ ) occurs for  $\lambda_p \geq 0.34$ . Therefore, it is possible to conclude that while for  $\lambda_p \leq 0.31$  the difference between  $\gamma_p$  and  $\gamma_{10}$  is significant, for larger  $\lambda_p$  the difference becomes small, i.e., the height does not play a large role anymore. Around  $\lambda_p = 0.33$ , an abrupt decrease of  $\gamma_p$  and  $\gamma_{10}$  as a function of  $\lambda_p$  takes place.  $\lambda_p = 0.33$  might therefore be interpreted as a critical value for the flow regime. This hypothesis is corroborated by the fact that  $\lambda_p = 0.33$  is close to  $\lambda_p = 0.35$ , i.e., the value of the plan area density that is

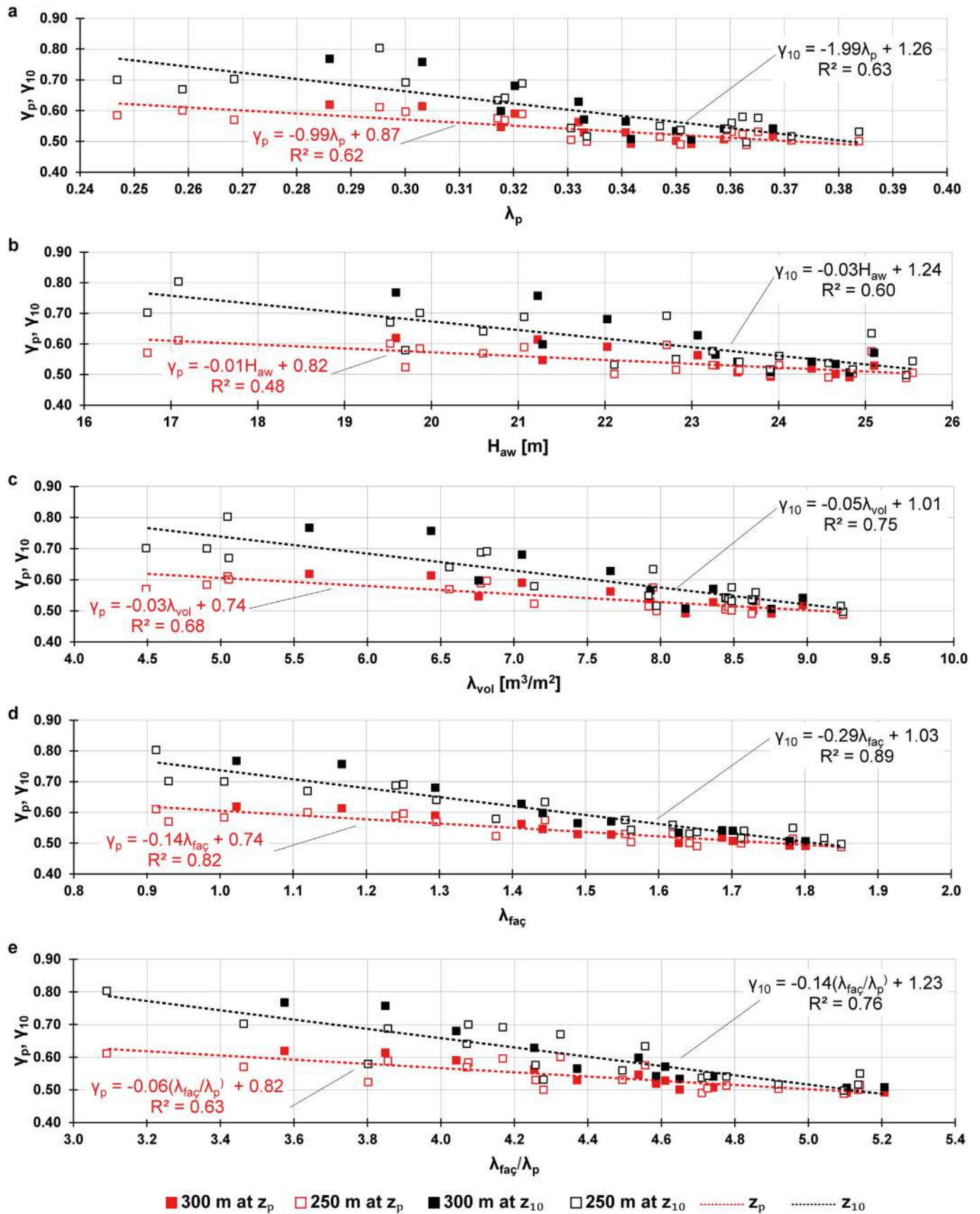


Fig. 8.  $\gamma_p$  and  $\gamma_{10}$  as a function of: (a) plan area density,  $\lambda_p$ ; (b) area-weighted mean building height,  $H_{aw}$ ; (c) volume density,  $\lambda_{vol}$ ; (d) façade area density,  $\lambda_{fac}$ ; and (e)  $\lambda_{fac}/\lambda_p$ .



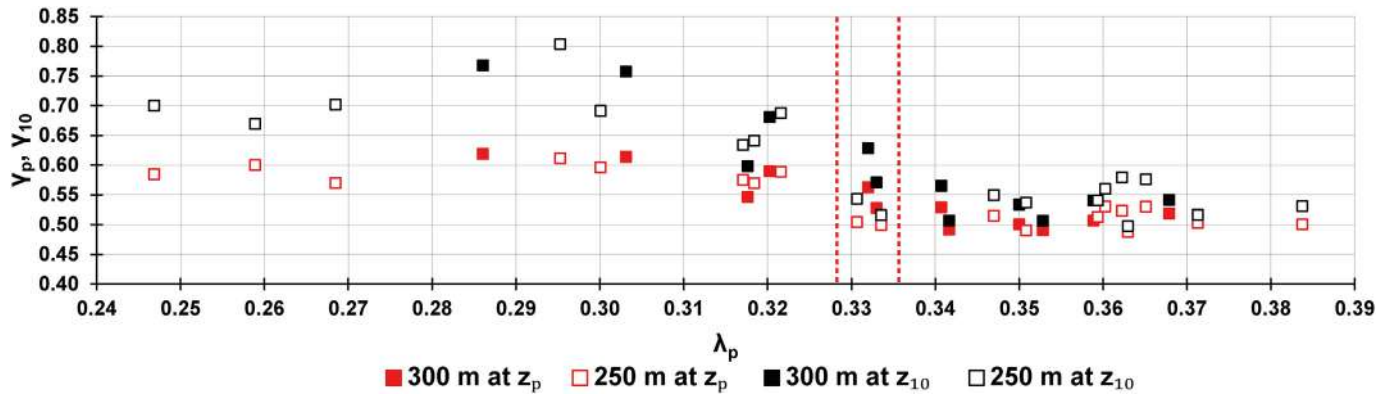


Fig. 9.  $\gamma_p$  versus  $\lambda_p$ . The dashed lines identify the possible range of variation of the critical value for the flow regime change, i.e., from the WIF to the SF regimes.

usually considered as the limit between the wake-interference flow (WIF) and the skimming flow (SF) regimes (Grimmond and Oke, 1999). Previous studies have demonstrated that in the WIF regime, the interaction between the buildings becomes evident (Lee and Soliman, 1977; Hussain and Lee, 1980; Oke, 1987; Oke, 1988). In fact, the buildings are close enough to each other so that their wakes and the vortices around their sharp edges cannot develop fully and interact with each other. Conversely, it has been demonstrated that in the SF regime, the building density is so large that approaching wind enters into the canyons with difficulties (Hussain and Lee, 1980). In the latter case, the flow skims over the roofs and stable vortices form in the space between buildings. As a result, in the SF regime outer and inner flows are decoupled to a large degree and vertical exchanges of mass and momentum are low. Therefore, the minimal difference between  $\gamma_p$  and  $\gamma_{10}$  for  $\lambda_p \geq 0.34$  may be explained as the consequence of the SF regime.

## 6. Limitations and future work

The scope of this investigation is the analysis of the impact of morphological parameters on the urban ventilation in real compact urban areas. The study is subjected to a number of limitations, which may be addressed in future research:

- Isothermal steady-state RANS simulations are performed to conduct the investigations. The inclusion of thermal effects obtained modelling solar radiation, long-wave radiation, convection and conduction should provide additional insights into the phenomenon. Unsteady RANS simulations may be used in a future study to investigate the diurnal variation of temperature and extend the study into the realm of thermal microclimate.
- The focus of this investigation is on real compact urban areas, which are characterized by a range of  $\lambda_p$  between 0.25 and 0.4 (Buccolieri et al., 2015; Chen et al., 2017; Mei et al., 2017). Future analyses should consider a  $\lambda_p$  range wider than that considered in this work (0.25 – 0.38) to investigate a broader variety of cases and to extend the range of building densities of the models provided.
- Guided “random” cases without taking into account the different building typologies have been considered in the present analysis. A further step could be to consider only areas of interest with homogeneous morphologies, quantifying also the role played by the single morphologies and building typologies in the urban ventilation.
- The goal of the study is to provide simple linear models for evaluating the urban ventilation performance at the early stages of the urban planning and building design processes. The urban

ventilation performance has been evaluated using the spatially averaged wVR that in the last decade has been proven as a useful indicator, in both idealized (Razak et al. (2013) and actual urban areas (Kubota et al., 2008). Nevertheless, further developments of the present work may be conducted using the other indicators and methodologies as presented in the literature review.

## 7. Summary and conclusion

This paper presents a study based on isothermal RANS simulations to investigate the impact of the morphology on the urban ventilation within a compact area in Rome, Italy. The investigated area is the Tuscolano-Don Bosco district representative of a compact city with a Mediterranean climate. Within the area, 31 AIs complying with three requirements are selected. The requirements imply constraints about the dimensions and the locations of the AIs. Morphological analyses have been carried out using the open-source GIS software QGIS. A set of seven MPs common among practitioners, policymakers and designers are employed to characterize the AIs quantitatively. This choice is motivated by a more general scope of the present study: an attempt to integrate different disciplines, i.e., on the one hand, building design and urban planning, and, on the other hand, wind engineering, in order to ease the management of the urban environment complexity. The AIs show different morphologies and a range of  $\lambda_p$  between 0.25 – 0.38. These values are in line with those found in the literature and corroborate the choice of Tuscolano-Don Bosco as a case study. Among the MPs, the relations  $\lambda_p$ - $\lambda_{vol}$  and  $\lambda_p$ - $\lambda_{fac}$  present strong correlations, i.e.,  $R^2 = 0.82$  and  $R^2 = 0.73$ , respectively, and may be used to characterize urban areas since they not only report quantities about the building density, volume and, façade but can also provide insights into the building typologies. Regarding the building height, a set of indices, e.g., mean building height ( $H_m$ ), root mean square of the building heights ( $H_\sigma$ ), median of the building heights ( $H_{med}$ ), area-weighted mean building height ( $H_{aw}$ ), may provide information about the characteristics of the area. However, the building height usually is regulated by codes, and, therefore, correlations with other MPs may be low, as in the present case. As indicators for evaluating the ventilation, two non-dimensional mean wind velocities are employed, i.e.,  $\gamma_p = U_p/U_{ref}$  at pedestrian level and  $\gamma_{10} = U_{10}/U_{ref}$  at half of the average UC height. These mean velocities are spatially averaged over each of the 31 AIs and the 12 wind directions considered for the simulations. They can be interpreted as the reduction in mean wind velocity caused by the urban canopy.

The following main conclusions can summarize the work:

- There is a clear dependency of the ventilation indicators on the selected morphological parameters; therefore, simple models obtained using linear regression analysis are derived for each MP- $\gamma_P$  and MP- $\gamma_{10}$  relation.
- There is a strong correlation between the building density,  $\lambda_P$ , on the one hand, and  $\gamma_P$  and  $\gamma_{10}$  on the other hand. The same holds for the volume density,  $\lambda_{vol}$ , and  $\gamma_P$  and  $\gamma_{10}$ , while a remarkable correlation is found for  $\lambda_{fac}$ - $\gamma_P$  and  $\lambda_{fac}$ - $\gamma_{10}$ .
- Among the four MPs related to the height of the buildings, the area-weighted mean building height,  $H_{aw}$ , shows the strongest influence on urban ventilation. Nevertheless, its influence is the weakest compared to the other selected MPs:  $\lambda_P$ ,  $\lambda_{vol}$ ,  $\lambda_{fac}$ , and  $\lambda_{fac}/\lambda_P$ .
- $\lambda_P = 0.33$  might be interpreted as a critical value for the flow regime change, i.e., from the WIF to the SF regimes.

Finally, the present methodology is proven to be suitable for evaluating the ventilation performance for urban areas characterized by different morphologies, dimensions and locations. The MPs adopted seem promising to be embedded in the wind environment description, in particular at the pedestrian level. In fact, once the reference velocity is known (e.g., the one measured at the airport weather station closest to the considered site), the linear equations

for  $\gamma_P$  yield an estimate of the mean wind speed at the pedestrian level without any need to run the simulation. This characteristic makes the parameters suitable for urban ventilation assessment in the early stages of the design process. Therefore, the provided linear models can be valuable tools for practitioners, urban designers, and policymakers, particularly during the first stage of urban regeneration planning, for highlighting areas potentially vulnerable to poor air conditions without running computationally expensive simulations.

#### CRedit authorship contribution statement

**Olga Palusci:** Conceptualization, Data curation, Formal analysis, Investigation, Methodology, Software, Validation, Visualization, Writing – original draft, Writing – review & editing. **Paolo Monti:** Investigation, Methodology, Writing – review & editing. **Carlo Cecere:** Writing – review & editing, Supervision. **Hamid Montazeri:** Investigation, Methodology, Writing – review & editing. **Bert Blocken:** Investigation, Methodology, Writing – review & editing.

#### Declaration of competing interest

The authors declare that they have no known competing financial interests or personal relationships that could have appeared to influence the work reported in this paper.

## Appendix A

### A.1. Sub-configuration validation

Validation is fundamental to demonstrate the accuracy and reliability of CFD results. In the present work, the “sub-configuration validation procedure” has been employed. This procedure entails the identification of simplified test cases that include the salient features of the actual problem of interest (Oberkamp et al., 2004; Franke et al., 2007; Blocken et al., 2012). Since the focus of the study about the actual urban area is on mean wind velocity at different heights within urban canyons, the validation study should be performed using sub-configurations that provide experimental results at several locations at different heights within the urban canyon. For this purpose, the work by Soulhac et al. (2009) is selected.

### A.2. Wind-tunnel experiments

The CFD validation study is carried out using the wind tunnel (WT) measurements provided by Soulhac et al. (2009) who performed an experimental investigation on the complex flow patterns within street intersections. The experiments were conducted in the closed-circuit atmospheric boundary layer WT of the Laboratoire de Mécanique des Fluides et d'Acoustique (LMFA) at the Ecole Centrale de Lyon, France. The WT has a rectangular cross-section of 3.7 m in width and 2.5 m in height with a length of 14 m. The urban geometrical model used in the experiments was composed of 16 parallelepipeds (0.5 m × 0.5 m in plan and height,  $H$ , equal to 0.1 m) placed with a constant spacing ( $S = 0.1$  m) and representative of an urban arrangement where streets intersect each other orthogonally (Fig. A.1a). This configuration generated UCs with  $AR = 1$  and length  $L = 5H$ . The 1:200 reduced-scale building models corresponded to buildings of 100 m × 100 m × 20 m in full scale. Therefore, the modeled urban arrangement could be considered as representative of the real case study in terms of  $AR (= 1)$ , mean building height ( $= 20$  m), size of the islands and orthogonal arrangement. Irwin spires and roughness elements distributed over the upstream fetch of the test section were used in order to generate a neutrally stratified, turbulent boundary layer. The approach-flow profile of the mean velocity was nearly logarithmic:

$$U(z) = \frac{u_*}{\kappa} \ln \left( \frac{z-d}{z_0} \right) \quad (A.1)$$

where  $\kappa = 0.42$  is the von Karman constant,  $z$  the vertical coordinate,  $u_* = 0.27$  m/s the friction velocity,  $d = 0.02$  m the displacement height, and  $z_0 = 0.0027$  m the aerodynamic roughness length.

The velocity components along the streamwise and vertical ( $z$ -axis) directions were measured at five transversal ( $y$ -axis) locations ( $y_1 = -0.6H$ ,  $y_2 = -0.8H$ ,  $y_3 = -1.4H$ ,  $y_4 = -2.2H$ ,  $y_5 = -3H$ ) along the second canyon using a two-component Laser Doppler Anemometry system (Fig. A.1a, b). Further details on the experimental set-up and flow characteristics can be found in Soulhac et al. (2009).

### A.3. Computational model and grid-convergence study

The computational domain has dimensions  $L_D \times W_D \times H_D = 4.3 \times 3.7 \times 2.5$  m<sup>3</sup>. The cross-section of the domain is equal to the cross-section of the WT in accordance with the experimental set-up (Fig. A.1a, c). Therefore, the domain height is 25H. The roughness elements distributed



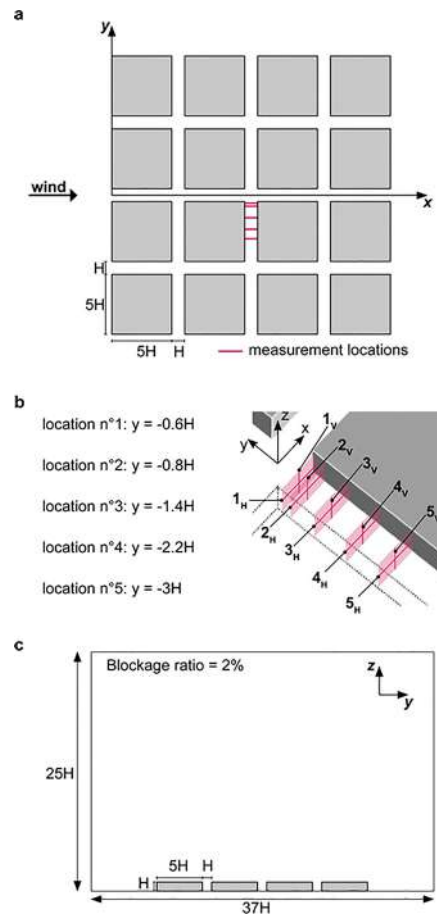


**Fig. A.1.** (a) Planar view of the model set-up, (b) parallel view of part of the model with the measurement locations, and (c) wind-tunnel cross section.

over the floor of the wind tunnel upwind of the parallelepipeds are not modeled explicitly, and the inlet and outlet planes were located  $5H$  upwind and  $15H$  downwind of the city model, respectively, according to best practice guidelines (Franke et al., 2007; Tominaga et al., 2008) (Fig. A.2a).

For the grid-convergence study, three computational grids are generated according to the best practice guidelines (Franke et al., 2007; Tominaga et al., 2008; Schatzmann et al., 2010; Blocken, 2015) and using the surface grid extrusion technique (van Hooff and Blocken, 2010). The basic grid is

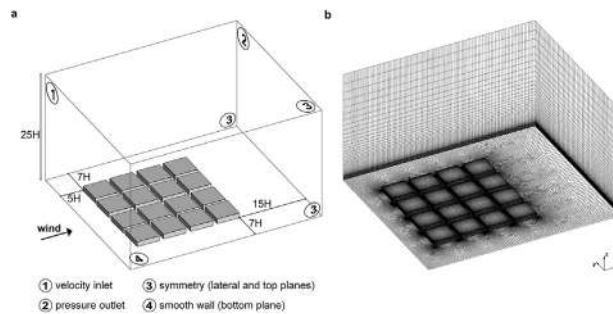


**Fig. A.2.** (a) Computational domain with indication of boundary condition types and (b) computational grid (basic case).

built with 40 cells along every building edge in plan view and 16 cells along the building height and building separation for a total of about  $3 \times 10^6$  hexahedral cells. The coarse and the fine grids are generated by the application of  $1/\sqrt{2}$  and  $\sqrt{2}$  linear factors to the grid resolution, respectively. The characteristics of the grids are listed in Table A.1 and the resulting grids are shown in Fig. A.3a-c.

**Table A.1**

Characteristics of the three grids for the grid-convergence study.

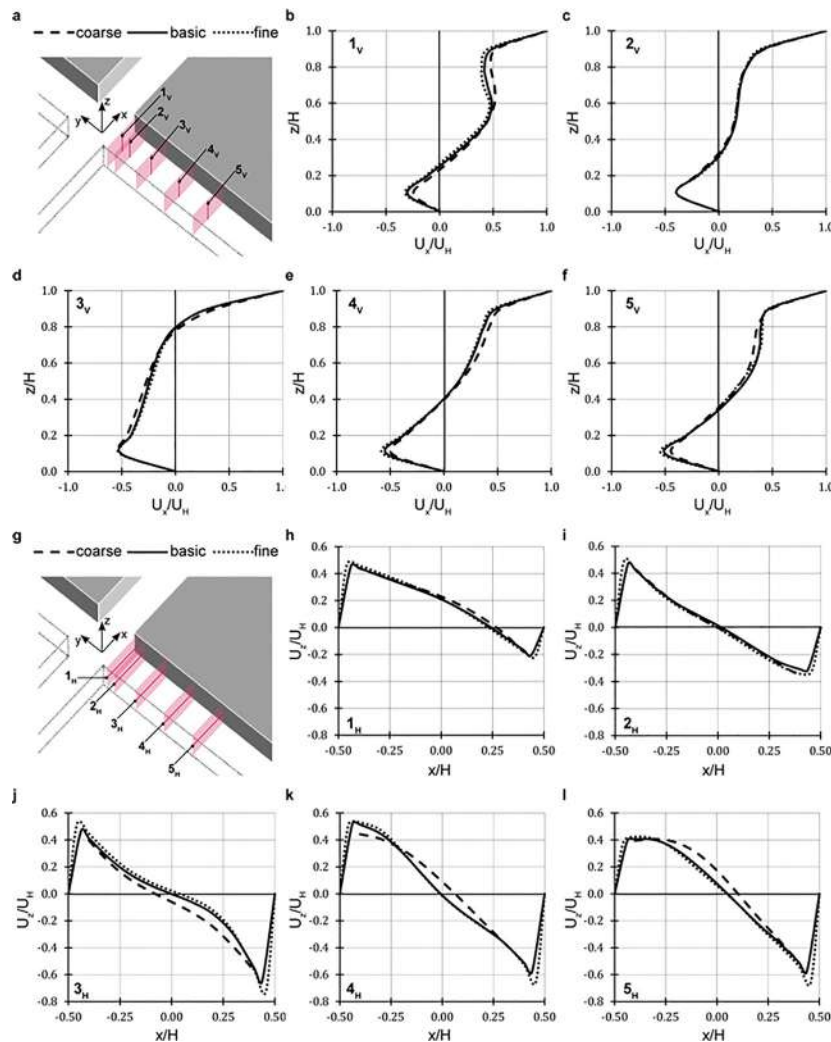
	Linear scale factor	Number of cells			
		Building edge (plan)	Building height	Building separation	Total
Coarse	$1/\sqrt{2}$	28	11	11	1,040,358
Basic	–	40	16	16	3,093,542
Fine	$\sqrt{2}$	57	23	23	6,324,237



Fig. A.4 compares the results on the three grids in terms of the non-dimensional mean streamwise,  $U_x/U_H$ , and vertical,  $U_z/U_H$ , velocity components.  $U_H$  is the mean, streamwise velocity at  $z = H$ . These comparisons are conducted along five vertical profiles (Fig. A.4b–f) and five horizontal lines (Fig. A.4h–l). The vertical lines ( $1_v$ ,  $2_v$ ,  $3_v$ ,  $4_v$ , and  $5_v$ ) belong to the central vertical plane passing through the main axis of the urban canyon of interest, while the horizontal lines ( $1_H$ ,  $2_H$ ,  $3_H$ ,  $4_H$ , and  $5_H$ ) are placed at  $z = 0.5H$ . It is apparent that the basic and the fine grids provide similar results along all five lines. Nevertheless, slight deviations of  $U_x/U_H$  and  $U_z/U_H$  occur at location  $y_1$  close to the top of the canyon, and at locations  $y_3$  and  $y_4$  close to the leeward façade, respectively. Conversely, significant deviations for both  $U_x/U_H$  and  $U_z/U_H$  occur between the coarse and the basic grids at different positions. In order to provide a quantitative error estimation, the grid-convergence index (GCI) is used (Roache, 1997):

$$GSI_{basic} = F_s \times \left| \frac{r^p \times \left( \frac{U_{basic}}{U_H} - \frac{U_{fine}}{U_H} \right)}{(1 - r^p)} \right| \quad (A.2)$$

where  $r = \sqrt{2}$  is the linear grid refinement factor,  $p = 2$  is the formal order of accuracy and refers to the second-order discretization schemes used for the simulations, while  $F_s = 1.25$  is the safety factor, recommended when three grids are considered (Roache, 1997). The GCI values obtained for both  $U_x/U_H$  and  $U_z/U_H$  averaged over all data points along the ten lines are listed in Table A.2. Overall, the deviations are well below 5% along all the ten lines except at  $y_1$  for  $U_x/U_H$  and at  $y_3$  for  $U_z/U_H$ , where the deviations are close to 6%. A further refinement of the grid



**Fig. A.4.** (a, g) Part of the computational model showing the five measurement locations; vertical (b–f) and horizontal (h–l) profiles of  $U_x/U_H$  and  $U_z/U_H$  computed using the three grids at five different positions in the second canyon perpendicular to the wind direction.

has been conducted applying a scale factor of  $\sqrt{2}$  on the number of cells of every edge of the fine grid for a total number of hexahedral cells above  $14 \times 10^6$ . The results show slight improvements at every position of about 1%. Since this improvement is not significant compared to the increase in computational time, it is concluded that the basic grid provides nearly grid-independent results, and it is retained for the validation study.

**Table A.2**

Grid Convergence Index (GCI) evaluated for the basic grid. Averages of  $U_x/U_H$  and  $U_z/U_H$  over all data points along the ten lines.

GCI <sub>basic</sub>	$Y_1$ −0.6 H	$Y_2$ −0.8 H	$Y_3$ −1.4 H	$Y_4$ −2.2 H	$Y_5$ −3 H
$U_x/U_H$	0.06	0.02	0.03	0.03	0.04
$U_z/U_H$	0.02	0.05	0.06	0.02	0.04

#### A.4. Boundary conditions and solver settings

The vertical profiles of mean wind speed,  $U$ , turbulence kinetic energy,  $k$  ( $\text{m}^2/\text{s}^2$ ), and turbulence dissipation rate,  $\varepsilon$  ( $\text{m}^2/\text{s}^3$ ), are imposed at the inlet plane. In particular, Eqn A.1 is used for  $U$ , while  $k$  and  $\varepsilon$  are given by:

$$k(z) = \frac{(u_*')^2}{\sqrt{C_\mu}} \quad (\text{A.3})$$

$$\varepsilon(z) = \frac{(u_*')^3}{\kappa(Z + Z_0)} \quad (\text{A.4})$$

where  $C_\mu = 0.09$  is a constant. At the top and lateral sides of the domain, symmetry boundary conditions, i.e., zero normal velocity and zero normal gradients of all variables, are applied (Fig. A.2a). At the outlet section, zero static gauge pressure is imposed. Moreover, for the bottom and building surfaces, the standard wall functions by Launder and Spalding (1974) with roughness modification by Cebeci and Bradshaw (1977) are used imposing zero roughness height, i.e.  $k_s = 0$  and  $C_s = 0.5$ .

The CFD simulations are performed applying the 3D steady RANS equations with the realizable (RE)  $k$ - $\varepsilon$  model closure (Shih et al., 1995) using Ansys Fluent 16.2 (ANSYS FLUENT 15.0, 2013). Although LES, when applied with care, is intrinsically superior to steady RANS, the latter approach is still most widely used in building simulation studies such as those on urban ventilation (Blocken, 2018). The SIMPLE algorithm is used for pressure-velocity coupling, while second-order discretization schemes are applied for both the convection and viscous terms of the

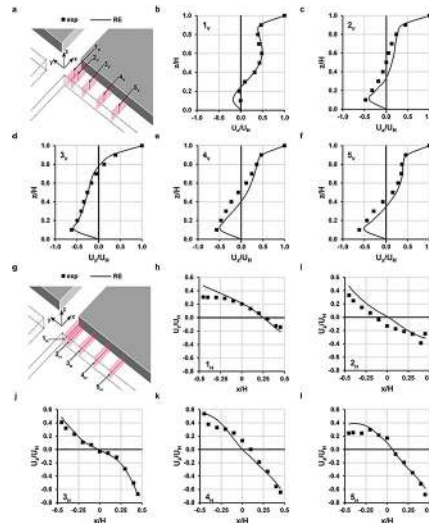


**Fig. A.5.** (a, g) Part of the computational model showing the five measurement locations; comparison between the wind tunnel data and the CFD results in terms of dimensionless  $U_x/U_H$  and  $U_z/U_H$  along (b-f) five vertical lines and (h-l) five horizontal lines respectively in the second canyon perpendicular to the wind direction.



governing equations. The choice for the realizable  $k-\epsilon$  turbulence model is based on the recommendations by Franke et al. (2004) and earlier successful validation studies with this model (Blocken et al., 2004; Blocken and Carmeliet, 2008; Blocken and Persoon, 2009; Blocken et al., 2012; Janssen et al., 2013; Toparlar et al., 2015; Antoniou et al., 2019). The simulations are terminated when the scaled residuals do not show any further reduction with an increasing number of iterations. The following minimum values are reached:  $10^{-5}$  for continuity,  $10^{-8}$  for  $x$ -,  $y$ -,  $z$ -velocity, and  $k$  and  $10^{-6}$  for  $\epsilon$ .

#### A.5. Results and validation

The results are presented in terms of non-dimensional mean streamwise,  $U_x/U_H$ , and vertical,  $U_z/U_H$ , velocity components, where  $U_H$  is the mean streamwise velocity at  $z = H$ . Fig. A.5 compare the CFD results in terms of  $U_x/U_H$  and  $U_z/U_H$  with the experimental data along five vertical lines ( $1_v$ ,  $2_v$ ,  $3_v$ ,  $4_v$ , and  $5_v$ ) belonging to the central vertical plane passing through the main axis of the urban canyon of interest and five horizontal lines ( $1_H$ ,  $2_H$ ,  $3_H$ ,  $4_H$ , and  $5_H$ ) placed at  $z = 0.5H$ . Overall, a reasonable agreement between the CFD simulations and WT data is found for both  $U_x/U_H$  and  $U_z/U_H$ . In particular, numerical and experimental  $U_x/U_H$  are very similar along lines  $1_v$  (apart from the bottom) and  $3_v$ , while slight deviations are present along lines  $2_v$  and  $4_v$ , especially in the central areas. A much more evident deviation is found for  $U_z/U_H$  along line  $2_H$ , while the agreement is satisfactory along lines  $1_H$ ,  $3_H$ , and  $5_H$ , even if slight differences occur close to the leeward facades ( $1_H$  and  $5_H$ ).

The validation metrics usually employed to quantitatively evaluate the computational settings are (Schatzmann et al., 2010) the hit rate ( $q$ ), the factor of 2 of the observations (FAC2), and the factor of 1.3 of the observations (FAC1.3):

$$q = \frac{N}{n} = \frac{1}{n} \sum_{i=1}^n N_i \text{ with } N_i = \begin{cases} 1 & \text{for } \left| \frac{P_i - O_i}{O_i} \right| \leq D \\ 0 & \text{else} \end{cases} \quad (\text{A.5})$$

$$\text{FAC2} = \frac{N}{n} = \frac{1}{n} \sum_{i=1}^n N_i \text{ with } N_i = \begin{cases} 1 & \text{for } 0.5 \leq \frac{P_i}{O_i} \leq 2.0 \\ 0 & \text{else} \end{cases} \quad (\text{A.6})$$

$$\text{FAC1.3} = \frac{N}{n} = \frac{1}{n} \sum_{i=1}^n N_i \text{ with } N_i = \begin{cases} 1 & \text{for } 0.77 \leq \frac{P_i}{O_i} \leq 1.3 \\ 0 & \text{else} \end{cases} \quad (\text{A.7})$$

where  $P_i$  is the predicted value (CFD),  $O_i$  is the observed value (WT) and  $n$  is the number of comparison points. An allowed fractional deviation  $D = 0.25$  is chosen for calculating  $q$  (VDI, 2005). The results show that the best performances in terms of both  $U_x/U_H$  and  $U_z/U_H$  occur at locations  $y_1$ ,  $y_3$ , and  $y_5$  (Table A.3). A reasonable agreement occurs at location  $y_4$ , while the worst agreement takes place along lines  $2_v$  and  $2_H$ .

**Table A.3**

Validation metrics for  $U_x/U_H$  and  $U_z/U_H$  along five vertical and horizontal lines in the second canyon perpendicular to the wind direction: hit rate, FAC2 - factor of two observations; FAC1.3 - factor of 1.3 observations.

	$U_x/U_H$					$U_z/U_H$					Average values	Ideal values
	$1_v$	$2_v$	$3_v$	$4_v$	$5_v$	$1_H$	$2_H$	$3_H$	$4_H$	$5_H$		
$q$	0.8	0.4	0.8	0.5	0.6	0.4	0.3	0.7	0.5	0.7	0.6	1.0
FAC2	0.8	0.6	0.8	0.7	0.8	0.9	0.6	0.9	0.8	0.9	0.8	1.0
FAC1.3	0.8	0.5	0.8	0.6	0.6	0.5	0.4	0.9	0.6	0.7	0.6	1.0

Since the average value of  $q$  is 0.6 and FAC2 is 0.8 (well above 0.5 as prescribed by Schatzmann et al., 2010), it can be concluded that the agreement between CFD simulations and WT data is satisfactory.

Moreover, a comparison between the performance of the RE  $k-\epsilon$  model and other turbulence models commonly used for urban wind flow simulations (Blocken, 2018), i.e., the standard  $k-\epsilon$  model (STD) (Jones and Launder, 1972), and the Renormalization Group  $k-\epsilon$  model (RNG) (Yakhot and Orszag, 1986), is conducted. The validation metrics used for assessing the performance are reported in Table A.4, and the comparison is presented in Fig. A.6. The results obtained using the STD  $k-\epsilon$  model and the RE  $k-\epsilon$  model are comparable, while the RNG  $k-\epsilon$  model shows an overall performance slightly worse. Therefore, the choice of the turbulence model closure may be considered validated. The current validation study is used to support the CFD simulations for the case study of the Tuscolano-Don Bosco district.

**Table A.4**

Validation metrics for  $U_x/U_H$  and  $U_z/U_H$  along five vertical and horizontal lines in the second canyon perpendicular to the wind direction:  $q$  - hit rate, FAC2 - factor of two observations; FAC1.3 - factor of 1.3 observations.

	$U_x/U_H$					$U_z/U_H$					Average values	Ideal values
	$1_v$	$2_v$	$3_v$	$4_v$	$5_v$	$1_H$	$2_H$	$3_H$	$4_H$	$5_H$		
$q$												
RE	0.80	0.40	0.80	0.50	0.60	0.36	0.27	0.73	0.45	0.73	0.56	1.0
STD	0.80	0.40	1.00	0.50	0.60	0.36	0.27	0.36	0.64	0.64	0.56	1.0
RNG	0.40	0.40	0.50	0.50	0.50	0.18	0.36	0.27	0.64	0.45	0.42	1.0
FAC 2												
RE	0.80	0.60	0.80	0.70	0.80	0.91	0.64	0.91	0.82	0.91	0.79	1.0
STD	0.90	0.70	1.00	0.80	0.80	0.82	0.64	0.91	0.91	0.91	0.84	1.0
RNG	0.90	0.70	1.00	0.70	0.90	0.64	0.64	0.82	0.73	0.91	0.79	1.0

(continued on next page)

Table A.4 (continued)

	$U_x/U_H$					$U_z/U_H$					Average values	Ideal values
	$1_V$	$2_V$	$3_V$	$4_V$	$5_V$	$1_H$	$2_H$	$3_H$	$4_H$	$5_H$		
FAC 1.3												
RE	0.80	0.50	0.80	0.60	0.60	0.45	0.36	0.91	0.55	0.73	0.63	1.0
STD	0.80	0.40	1.00	0.60	0.60	0.27	0.27	0.45	0.64	0.64	0.57	1.0
RNG	0.50	0.40	0.50	0.50	0.50	0.27	0.27	0.36	0.64	0.45	0.44	1.0

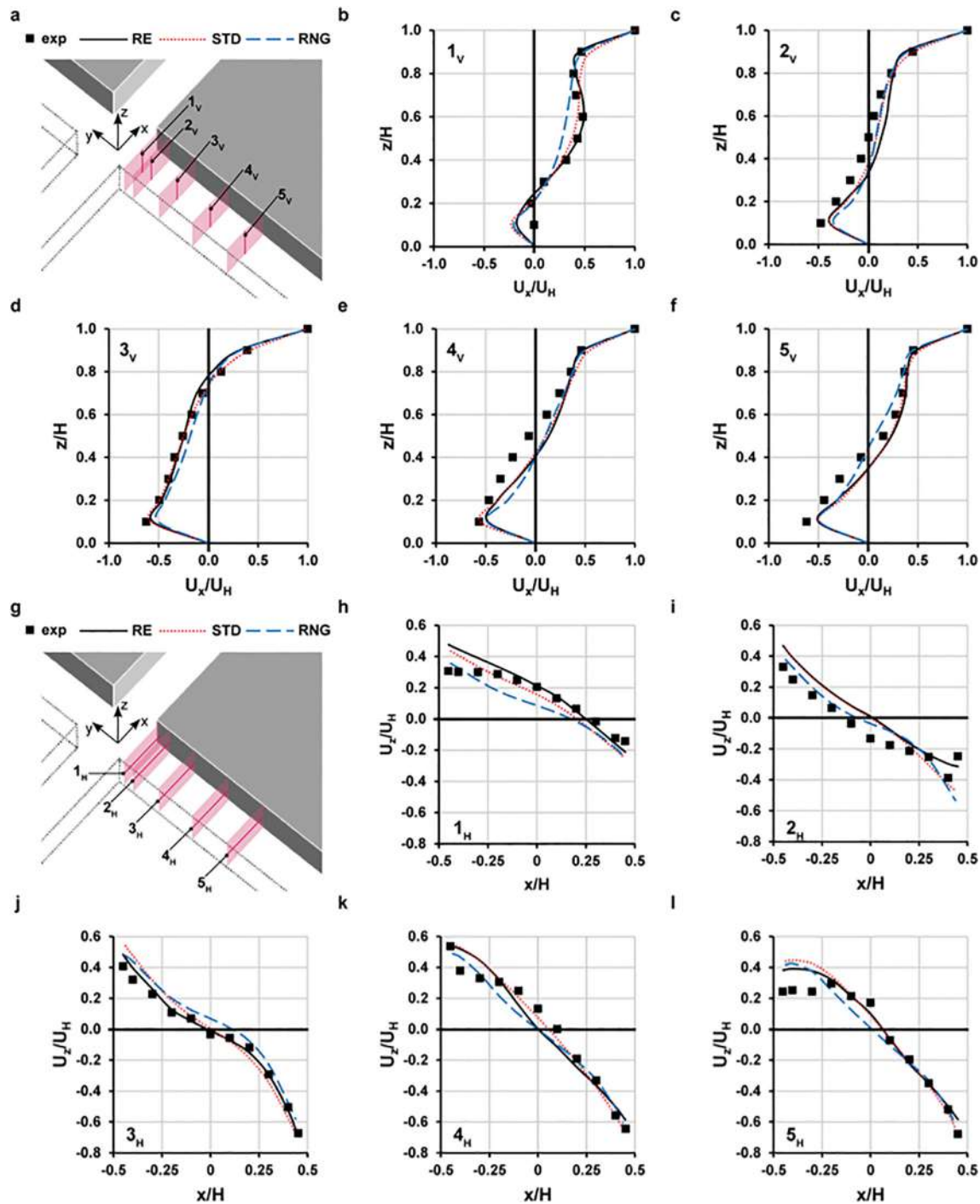
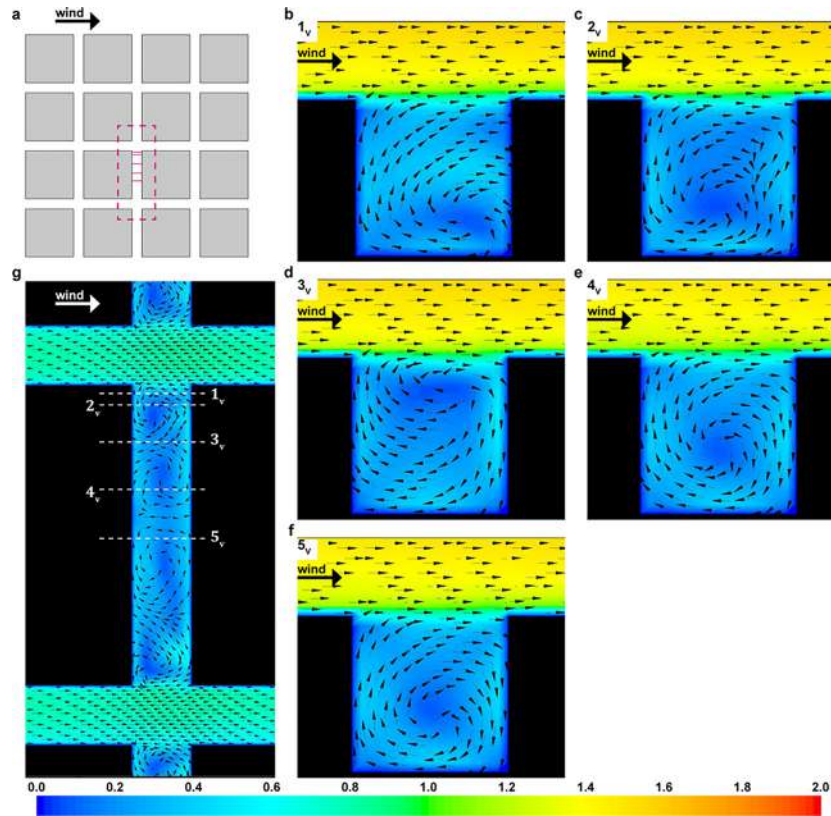


Fig. A.6. (a, g) Part of the computational model showing the five measurement locations; comparison between the wind tunnel data and the CFD results in terms of dimensionless  $U_x/U_H$  and  $U_z/U_H$  along (b-f) five vertical lines and (h-l) five horizontal lines respectively in the same canyon perpendicular to the wind direction. The CFD results are obtained with the RE k- $\epsilon$  model (black line), STD k- $\epsilon$  model (red dotted line), and RNG k- $\epsilon$  model (blue dashed line).



Finally, the mean velocity vector fields and non-dimensional mean velocity contours ( $U/U_{\text{ref}}$ , where  $U_{\text{ref}}$  is mean velocity at the inlet at  $z = 0.5H$  height) along the vertical planes passing through the  $1_v$ ,  $2_v$ ,  $3_v$ ,  $4_v$ , and  $5_v$  lines and along the horizontal plane at  $z = 0.5H$  are shown in Fig. A.7b–g, respectively. In the vertical planes, a main clockwise vortex is observed inside the canyon. Such a pattern is typically observed in the skimming flow regime when the wind flow overlaying the canopy skims over the top of buildings. However, contrary to the patterns typically observed in two-dimensional UCs (Salizzoni et al., 2011; Di Bernardino et al., 2018), the main vortex is not centered in the cavity, but follows the pattern generally occurring for medium-length UC ( $L/H = 5$ ) with  $AR = 1$  (Hunter et al., 1990). The center of the vortex changes its position (from the bottom of the windward façade to the center, to the top, to the center again) as we consider planes located increasingly towards the middle of the canyon. This characteristic reveals the 3D nature of the vortex that is not circular in a plane but helicoidal inside the entire canyon. In fact, counter-rotating vortices can be seen in the horizontal plane (Fig. A.7g).



**Fig. A.7.** (a) Top view of the model; vector fields and contours of the dimensionless mean velocity ( $U_{\text{ref}}$  at the inlet at  $z = 0.5H$  height) along (b–f) five vertical planes and (g) the horizontal plane at  $z = 0.5H$  height. Color bar refers to the dimensionless velocity.

## Appendix B

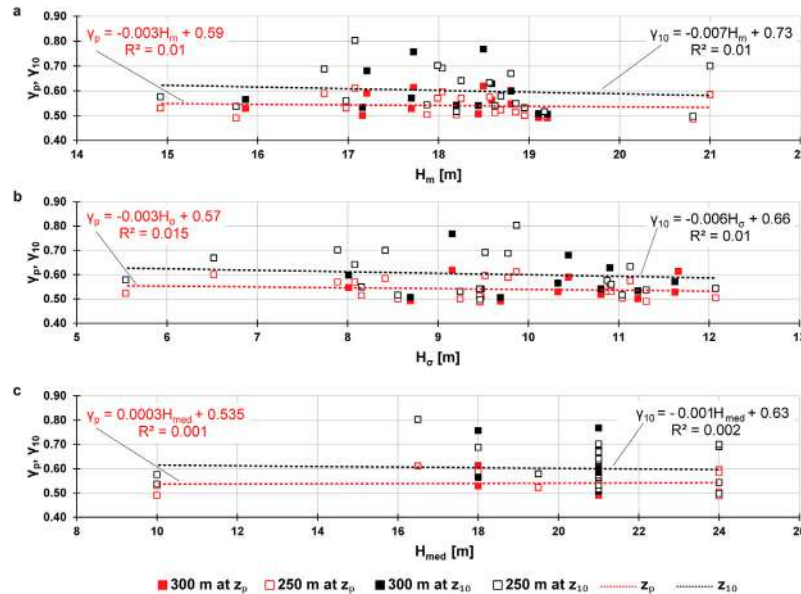


Fig. B.1.  $\gamma_p$  and  $\gamma_{10}$  as a function of: (a) mean building height,  $H_m$ ; (b) root mean square of the building heights,  $H_o$ ; and (c) median of the building heights ( $H_{med}$ ).

## References

- Ai, Z.T., Mak, C.M., 2017. CFD simulation of flow in a long street canyon under a perpendicular wind direction: evaluation of three computational settings. *Build. Environ.* 114, 293–306. <https://doi.org/10.1016/j.buildenv.2016.12.032>.
- Amicarelli, A., Salizzoni, P., Leuzzi, G., Monti, P., Soulhac, L., Cierco, F.X., Leboeuf, F., 2012. Sensitivity analysis of a concentration fluctuation model to dissipation rate estimates. *Int. J. Environ. Pollut.* 48, 164–173. <https://doi.org/10.1504/IJEP.2012.049663>.
- An, K., Fung, J.C.H., Yim, S.H.L., 2013. Sensitivity of inflow boundary conditions on downstream wind and turbulence profiles through building obstacles using a CFD approach. *J. Wind Eng. Ind. Aerodyn.* 115, 137–149. <https://doi.org/10.1016/j.jweia.2013.01.004>.
- ANSYS FLUENT 15.0, 2013. *ANSYS Fluent Theory Guide*. 15317. ANSYS Inc, USA, pp. 724–746.
- Antoniou, N., Montazeri, H., Wigo, H., Neophytou, M.K.A., Blocken, B., Sandberg, M., 2017. CFD and wind-tunnel analysis of outdoor ventilation in a real compact heterogeneous urban area: evaluation using “air delay”. *Build. Environ.* 126, 355–372. <https://doi.org/10.1016/j.buildenv.2017.10.013>.
- Antoniou, N., Montazeri, H., Neophytou, M., Blocken, B., 2019. CFD simulation of urban microclimate: validation using high-resolution field measurements. *Sci. Total Environ.* 695, 133743. <https://doi.org/10.1016/j.scitotenv.2019.133743>.
- Ashie, Y., Kono, T., 2011. Urban-scale CFD analysis in support of a climate-sensitive design for the Tokyo Bay area. *Int. J. Climatol.* 31, 174–188. <https://doi.org/10.1002/joc.2226>.
- Badas, M.G., Ferrari, S., Garau, M., Querzoli, G., 2017. On the effect of gable roof on natural ventilation in two-dimensional urban canyons. *J. Wind Eng. Ind. Aerodyn.* 162, 24–34. <https://doi.org/10.1016/j.jweia.2017.01.006>.
- Bady, M., Kato, S., Huang, H., 2008. Towards the application of indoor ventilation efficiency indices to evaluate the air quality of urban areas. *Build. Environ.* 43, 1991–2004. <https://doi.org/10.1016/j.buildenv.2007.11.013>.
- Bady, M., Kato, S., Takahashi, T., Huang, H., 2011. An experimental investigation of the wind environment and air quality within a densely populated urban street canyon. *J. Wind Eng. Ind. Aerodyn.* 99, 857–867. <https://doi.org/10.1016/j.jweia.2011.06.005>.
- Bentham, T., Britter, R.E., 2003. Spatially averaged flow within obstacle arrays. *Atmos. Environ.* 37, 2037–2043. [https://doi.org/10.1016/S1352-2310\(03\)00123-7](https://doi.org/10.1016/S1352-2310(03)00123-7).
- Berghauser Pont, M., Haupt, P., 2009. Space, Density and Urban Form. Ploughshares. Technische Universiteit Delft <https://doi.org/10.2307/20632013>.
- Blocken, B., 2014. 50 years of computational wind engineering: past, present and future. *J. Wind Eng. Ind. Aerodyn.* 129, 69–102. <https://doi.org/10.1016/j.jweia.2014.03.008>.
- Blocken, B., 2015. Computational fluid dynamics for urban physics: importance, scales, possibilities, limitations and ten tips and tricks towards accurate and reliable simulations. *Build. Environ.* 91, 219–245. <https://doi.org/10.1016/j.buildenv.2015.02.015>.
- Blocken, B., 2018. LES over RANS in building simulation for outdoor and indoor applications: a foregone conclusion? *Build. Simul.* 11, 821–870. <https://doi.org/10.1007/s12273-018-0459-3>.
- Blocken, B., Carmeliet, J., 2008. Pedestrian wind conditions at outdoor platforms in a high-rise apartment building: generic sub-configuration validation, wind comfort assessment and uncertainty issues. *Wind Struct. An Int. J.* 11, 51–70. <https://doi.org/10.12989/was.2008.11.1.051>.
- Blocken, B., Persoon, J., 2009. Pedestrian wind comfort around a large football stadium in an urban environment: CFD simulation, validation and application of the new dutch wind nuisance standard. *J. Wind Eng. Ind. Aerodyn.* 97, 255–270. <https://doi.org/10.1016/j.jweia.2009.06.007>.
- Blocken, B., Roels, S., Carmeliet, J., 2004. Modification of pedestrian wind comfort in the silvertop tower passages by an automatic control system. *J. Wind Eng. Ind. Aerodyn.* 92, 849–873. <https://doi.org/10.1016/j.jweia.2004.04.004>.
- Blocken, B., Stathopoulos, T., Carmeliet, J., 2007. CFD simulation of the atmospheric boundary layer: wall function problems. *Atmos. Environ.* 41, 238–252. <https://doi.org/10.1016/j.atmosenv.2006.08.019>.
- Blocken, B., Janssen, W.D., van Hooff, T., 2012. CFD simulation for pedestrian wind comfort and wind safety in urban areas: general decision framework and case study for the Eindhoven university campus. *Environ. Model. Softw.* 30, 15–34. <https://doi.org/10.1016/j.envsoft.2011.11.009>.
- Blocken, B., Vervoort, R., van Hooff, T., 2016. Reduction of outdoor particulate matter concentrations by local removal in semi-enclosed parking garages: a preliminary case study for Eindhoven city center. *J. Wind Eng. Ind. Aerodyn.* 159, 80–98. <https://doi.org/10.1016/j.jweia.2016.10.008>.
- Britter, R.E., Hanna, S.R., 2000. Flow and dispersion in urban areas. *Annu. Rev. Phys. Chem.* 51, 275–296. <https://doi.org/10.1146/annurev.physchem.51.1.275>.
- Bu, Z., Kato, S., Ishida, Y., Huang, H., 2009. New criteria for assessing local wind environment at pedestrian level based on exceedance probability analysis. *Build. Environ.* 44, 1501–1508. <https://doi.org/10.1016/j.buildenv.2008.08.002>.
- Buccolieri, R., Sandberg, M., Di Sabatino, S., 2010. City breathability and its link to pollutant concentration distribution within urban-like geometries. *Atmos. Environ.* 44, 1894–1903. <https://doi.org/10.1016/j.atmosenv.2010.02.022>.
- Buccolieri, R., Salizzoni, P., Soulhac, L., Garbero, V., Di Sabatino, S., 2015. The breathability of compact cities. *Urban Clim.* 13, 73–93. <https://doi.org/10.1016/j.uclim.2015.06.002>.
- Buccolieri, R., Wigö, H., Sandberg, M., Di Sabatino, S., 2017. Direct measurements of the drag force over aligned arrays of cubes exposed to boundary-layer flows. *Environ. Fluid Mech.* 17, 373–394. <https://doi.org/10.1007/s10652-016-9493-9>.
- Cantelli, A., Monti, P., Leuzzi, G., 2015. Numerical study of the urban geometrical representation impact in a surface energy budget model. *Environ. Fluid Mech.* 15, 251–273. <https://doi.org/10.1007/s10652-013-9309-0>.
- Cárdenas Rodríguez, M., Dupont-Courtade, L., Oueslati, W., 2016. Air pollution and urban structure linkages: evidence from european cities. *Renew. Sust. Energ. Rev.* 53, 1–9. <https://doi.org/10.1016/j.rser.2015.07.190>.
- Carpentieri, M., Robins, A.G., 2015. Influence of urban morphology on air flow over building arrays. *J. Wind Eng. Ind. Aerodyn.* 145, 61–74. <https://doi.org/10.1016/j.jweia.2015.06.001>.
- Carta Tecnica Regionale, 2016. <http://dati.lazio.it/catalog/it/dataset/carta-tecnica-regionale-2002-2003-5k-roma/resource/ee089059-bdec-499c-a91c-a3f2a71f32ce>.
- Casey, M., Wintergerste, T., 2000. Best Practice Guidelines, ERCOFTAC Special Interest Group on Quality and Trust in Industrial CFD.
- Cebeci, T., Bradshaw, P., 1977. *Momentum Transfer in Boundary Layers*. Hemisphere Publishing Corp, New York, New York.



- Chen, L., Hang, J., Sandberg, M., Claesson, L., Sabatino, S.D., Wigo, H., 2017. The impacts of building height variations and building packing densities on flow adjustment and city breathability in idealized urban models. *Build. Environ.* <https://doi.org/10.1016/j.buildenv.2017.03.042>.
- Cheng, H., Castro, I.P., 2002. Near wall flow OVER URBAN-like roughness. *Bound.-Layer Meteorol.* 104, 229–259.
- Cheng, W.C., Liu, C.H., Leung, D.Y.C., 2008. Computational formulation for the evaluation of street canyon ventilation and pollutant removal performance. *Atmos. Environ.* 42, 9041–9051. <https://doi.org/10.1016/j.atmosenv.2008.09.045>.
- Cocael, O., Thomas, T.G., Castro, I.P., Belcher, S.E., 2006. Mean flow and turbulence statistics over groups of urban-like cubical obstacles. *Bound.-Layer Meteorol.* 121, 491–519. <https://doi.org/10.1007/s10546-006-9076-2>.
- Conigliaro, E., Monti, P., Leuzzi, G., Cantelli, A., 2021. A three-dimensional urban canopy model for mesoscale atmospheric simulations and its comparison with a two-dimensional urban canopy model in an idealized case. *Urban Clim.* 37, 100831. <https://doi.org/10.1016/j.uclim.2021.100831>.
- Di Bernardino, A., Monti, P., Leuzzi, G., Querzoli, G., 2017. Water-channel estimation of eulerian and lagrangian time scales of the turbulence in idealized two-dimensional urban canopies. *Bound.-Layer Meteorol.* 165, 251–276. <https://doi.org/10.1007/s10546-017-0278-6>.
- Di Bernardino, A., Monti, P., Leuzzi, G., Querzoli, G., 2018. Pollutant fluxes in two-dimensional street canyons. *Urban Clim.* 24, 80–93. <https://doi.org/10.1016/j.uclim.2018.02.002>.
- Di Bernardino, A., Monti, P., Leuzzi, G., Querzoli, G., 2020a. Turbulent Schmidt number measurements over three-dimensional cubic arrays. *Bound.-Layer Meteorol.* 174, 231–250. <https://doi.org/10.1007/s10546-019-00482-z>.
- Di Bernardino, A., Monti, P., Leuzzi, G., Querzoli, G., 2020b. Eulerian and lagrangian time scales of the turbulence above staggered arrays of cubical obstacles. *Environ. Fluid Mech.* 20, 987–1005. <https://doi.org/10.1007/s10652-020-09736-8>.
- Di Bernardino, A., Iannarelli, A.M., Casadio, S., Perrino, C., Barnaba, F., Tofful, L., Campanelli, M., Di Liberto, L., Mevi, G., Siani, A.M., Cacciani, M., 2021. Impact of synoptic meteorological conditions on air quality in three different case studies in Rome, Italy. *Atmos. Pollut. Res.* 12, 76–88. <https://doi.org/10.1016/j.apr.2021.02.019>.
- Di Bernardino, A., Palusci, O., Pini, A., Leuzzi, G., Cacciani, M., Pelliccioni, A., Monti, P., 2021. Air Circulation in Urban Areas. In: Palme, E., Salvati, A. (Eds.), *Urban Microclimate Modelling for Comfort and Energy Studies*. Springer International Publishing, pp. 195–221. <https://doi.org/10.1007/978-3-030-65421-4>.
- Di Sabatino, S., Buccolieri, R., Pulvirenti, B., Britter, R.E., 2007. Simulations of pollutant dispersion within idealised urban-type geometries with CFD and integral models. *Atmos. Environ.* 41, 8316–8329. <https://doi.org/10.1016/j.atmosenv.2007.06.052>.
- Du, Y., Mak, C.M., Kwok, K., Tse, K.T., Lee, T.Cheung, Ai, Z., Liu, J., Niu, J., 2017. New criteria for assessing low wind environment at pedestrian level in Hong Kong. *Build. Environ.* 123, 23–36. <https://doi.org/10.1016/j.buildenv.2017.06.036>.
- Du, Y., Mak, C.M., Li, Y., 2018. Application of a multi-variable optimization method to determine lift-up design for optimum wind comfort. *Build. Environ.* 131, 242–254. <https://doi.org/10.1016/j.buildenv.2018.01.012>.
- Du, Y., Mak, C.M., Li, Y., 2019. A multi-stage optimization of pedestrian level wind environment and thermal comfort with lift-up design in ideal urban canyons. *Sustain. Cities Soc.* 46, 101424. <https://doi.org/10.1016/j.scs.2019.101424>.
- Franke, J., Hirsch, C., Jensen, A.G., Krus, H.W., Schatzmann, M., Miles, P.S.W., S.D., Wisse, J.A., Wright, N.G., 2004. Recommendations on the Use of CFD in Wind Engineering. *Cost Action C*, pp. 1–11.
- Franke, J., Hellsten, A., Schlünzen, H., Carissimo, B., 2007. *Best Practice Guideline for the CFD Simulation of Flows in the Urban Environment*. COST Action.
- Gao, Z., Bresson, R., Qu, Y., Milliez, M., de Munck, C., Carissimo, B., 2018. High resolution unsteady RANS simulation of wind, thermal effects and pollution dispersion for studying urban renewal scenarios in a neighborhood of Toulouse. *Urban Clim.* 23, 114–130. <https://doi.org/10.1016/j.uclim.2016.11.002>.
- Gasparrini, A., Guo, Y., Hashizume, M., Lavigne, E., Zanobetti, A., Schwartz, J., Tobias, A., Tong, S., Rocklöv, J., Forsberg, B., Leone, M., De Sario, M., Bell, M.L., Guo, Y.-L.L., Wu, C., Kan, H., Yi, S.-M., Coelho, M.de S.Z.S., Saldiva, P.H.N., Honda, Y., Kim, H., Armstrong, B., 2015. Mortality risk attributable to high and low ambient temperature: a multicountry observational study. *Lancet* 386, 369–375. [https://doi.org/10.1016/S0140-6736\(14\)62114-0](https://doi.org/10.1016/S0140-6736(14)62114-0).
- Gousseau, P., Blocken, B., Stathopoulos, T., van Heijst, G.J.F., 2011. CFD simulation of near-field pollutant dispersion on a high-resolution grid: a case study by LES and RANS for a building group in downtown Montreal. *Atmos. Environ.* 45, 428–438. <https://doi.org/10.1016/j.atmosenv.2010.09.065>.
- Grimmond, C.S.B., Oke, T.R., 1999. Aerodynamic properties of urban areas derived from analysis of surface form. *J. Appl. Meteorol.* 38, 1262–1292.
- Gromke, C., Blocken, B., Janssen, W.D., Merema, B., van Hooff, T., Timmermans, H., 2015. CFD analysis of transpirational cooling by vegetation: Case study for specific meteorological conditions during a heat wave in Arnhem, Netherlands. *Build. Environ.* 83, 11–26. <https://doi.org/10.1016/j.buildenv.2014.04.022>.
- Hagishima, A., Tanimoto, J., Nagayama, K., Meno, S., 2009. Aerodynamic parameters of regular arrays of rectangular blocks with various geometries. *Bound.-Layer Meteorol.* 132, 315–337. <https://doi.org/10.1007/s10546-009-9403-5>.
- Hang, J., Li, Y., 2010. Ventilation strategy and air change rates in idealized high-rise compact urban areas. *Build. Environ.* 45, 2754–2767. <https://doi.org/10.1016/j.BUILDENV.2010.06.004>.
- Hang, J., Li, Y., 2011. Age of air and air exchange efficiency in high-rise urban areas and its link to pollutant dilution. *Atmos. Environ.* 45, 5572–5585. <https://doi.org/10.1016/j.atmosenv.2011.04.051>.
- Hang, J., Sandberg, M., Li, Y., 2009a. Effect of urban morphology on wind condition in idealized city models. *Atmos. Environ.* 43, 869–878. <https://doi.org/10.1016/j.atmosenv.2008.10.040>.
- Hang, J., Sandberg, M., Li, Y., 2009b. Age of air and air exchange efficiency in idealized city models. *Build. Environ.* 44, 1714–1723. <https://doi.org/10.1016/j.buildenv.2008.11.013>.
- Hang, J., Sandberg, M., Li, Y., Claesson, L., 2009c. Pollutant dispersion in idealized city models with different urban morphologies. *Atmos. Environ.* 43, 6011–6025. <https://doi.org/10.1016/j.atmosenv.2009.08.029>.
- Hang, J., Li, Y., Sandberg, M., Claesson, L., 2010a. Wind conditions and ventilation in high-rise long street models. *Build. Environ.* 45, 1353–1365. <https://doi.org/10.1016/j.BUILDENV.2009.11.019>.
- Hang, J., Sandberg, M., Li, Y., Claesson, L., 2010b. Flow mechanisms and flow capacity in idealized long-street city models. *Build. Environ.* 45, 1042–1053. <https://doi.org/10.1016/j.BUILDENV.2009.10.014>.
- Hang, J., Li, Y., Sandberg, M., 2011. Experimental and numerical studies of flows through and within high-rise building arrays and their link to ventilation strategy. *J. Wind Eng. Ind. Aerodyn.* 99, 1036–1055. <https://doi.org/10.1016/j.jweia.2011.07.004>.
- Hang, J., Li, Y., Buccolieri, R., Sandberg, M., Di Sabatino, S., 2012a. On the contribution of mean flow and turbulence to city breathability: the case of long streets with tall buildings. *Sci. Total Environ.* 416, 362–373. <https://doi.org/10.1016/j.scitotenv.2011.12.016>.
- Hang, J., Li, Y., Sandberg, M., Buccolieri, R., Di Sabatino, S., 2012b. The influence of building height variability on pollutant dispersion and pedestrian ventilation in idealized high-rise urban areas. *Build. Environ.* 56, 346–360. <https://doi.org/10.1016/j.buildenv.2012.03.023>.
- Hang, J., Luo, Z., Sandberg, M., Gong, J., 2013. Natural ventilation assessment in typical open and semi-open urban environments under various wind directions. *Build. Environ.* 70, 318–333. <https://doi.org/10.1016/j.buildenv.2013.09.002>.
- Hang, J., Wang, Q., Chen, X., Sandberg, M., Zhu, W., Buccolieri, R., Di Sabatino, S., 2015. City breathability in medium density urban-like geometries evaluated through the pollutant transport rate and the net escape velocity. *Build. Environ.* 94, 166–182. <https://doi.org/10.1016/j.buildenv.2015.08.002>.
- Ho, Y.-K., Liu, C.-H., Wong, M.S., 2015. Preliminary study of the parameterisation of street-level ventilation in idealised two-dimensional simulations. *Build. Environ.* 89, 345–355. <https://doi.org/10.1016/j.BUILDENV.2015.02.042>.
- Hu, T., Yoshie, R., 2013. Indices to evaluate ventilation efficiency in newly-built urban area at pedestrian level. *J. Wind Eng. Ind. Aerodyn.* 112, 39–51. <https://doi.org/10.1016/j.jweia.2012.11.002>.
- Huang, H., Kato, S., Ooka, R., Jiang, T., 2006. CFD analysis of ventilation efficiency around an elevated highway using visitation frequency and purging flow rate. *Wind Struct. An Int. J.* 9, 297–313.
- Hunter, L.J., Watson, I.D., Johnson, G.T., 1990. Modelling air flow regimes in urban canyons. *Energy Build.* 91, 15–16. [https://doi.org/10.1016/0378-7788\(90\)90004-3](https://doi.org/10.1016/0378-7788(90)90004-3).
- Hunter, L.J., Johnson, G.T., Watson, I.D., 1992. An investigation of three-dimensional characteristics of flow regimes within the urban canyon. *Atmos. Environ.* 26, 425–432. [https://doi.org/10.1016/0957-1272\(92\)90049-X](https://doi.org/10.1016/0957-1272(92)90049-X).
- Hussain, M., Lee, B.E., 1980. A wind tunnel study of the mean pressure forces acting on large groups of low-rise buildings. *J. Wind Eng. Ind. Aerodyn.* 6, 207–225. [https://doi.org/10.1016/0167-6105\(80\)90002-1](https://doi.org/10.1016/0167-6105(80)90002-1).
- Ikegaya, N., Ikeda, Y., Hagishima, A., Razak, A.A., Tanimoto, J., 2017. A prediction model for wind speed ratios at pedestrian level with simplified urban canopies. *Theor. Appl. Climatol.* 127, 655–665. <https://doi.org/10.1007/s00704-015-1655-z>.
- Iousef, S., Montazeri, H., Blocken, B., van Wesemael, P.J.V., 2017. On the use of non-conformal grids for economic LES of wind flow and convective heat transfer for a wall-mounted cube. *Build. Environ.* 119, 44–61. <https://doi.org/10.1016/j.buildenv.2017.04.004>.
- Janssen, W.D., Blocken, B., van Hooff, T., 2013. Pedestrian wind comfort around buildings: comparison of wind comfort criteria based on whole-flow field data for a complex case study. *Build. Environ.* 59, 547–562. <https://doi.org/10.1016/j.buildenv.2012.10.012>.
- Jeanjean, A.P.R., Buccolieri, R., Eddy, J., Monks, P.S., Leigh, R.J., 2017. Air quality affected by trees in real street canyons: the case of marylebone neighbourhood in Central London. *Urban For. Urban Green.* 22, 41–53. <https://doi.org/10.1016/j.UFUG.2017.01.009>.
- Jones, W.P., Launder, B.E., 1972. The prediction of laminarization with a two-equation model of turbulence. *Int. J. Heat Mass Transf.* 15, 301–314. [https://doi.org/10.1016/0017-9310\(72\)90076-2](https://doi.org/10.1016/0017-9310(72)90076-2).
- Juan, Y.H., Yang, A.S., Wen, C.Y., Lee, Y.T., Wang, P.C., 2017. Optimization procedures for enhancement of city breathability using arcade design in a realistic high-rise urban area. *Build. Environ.* 121, 247–261. <https://doi.org/10.1016/j.buildenv.2017.05.035>.
- Kanda, M., 2006. Large-eddy simulations on the effects of surface geometry of building arrays on turbulent organized structures. *Bound.-Layer Meteorol.* 118, 151–168. <https://doi.org/10.1007/s10546-005-5294-2>.
- Kato, S., Huang, H., 2009. Ventilation efficiency of void space surrounded by buildings with wind blowing over built-up urban area. *J. Wind Eng. Ind. Aerodyn.* 97, 358–367. <https://doi.org/10.1016/j.jweia.2009.05.003>.
- Kubota, T., Miura, M., Tominaga, Y., Mochida, A., 2008. Wind tunnel tests on the relationship between building density and pedestrian-level wind velocity: development of guidelines for realizing acceptable wind environment in residential neighborhoods. *Build. Environ.* 43, 1699–1708. <https://doi.org/10.1016/j.buildenv.2007.10.015>.
- Launder, B.E., Spalding, D.B., 1974. The numerical computation of turbulent flows. *Comput. Methods Appl. Mech. Eng.* 3, 269–289. [https://doi.org/10.1016/0045-7825\(74\)90029-2](https://doi.org/10.1016/0045-7825(74)90029-2).
- Lauriks, T., Longo, R., Baetens, D., Derudi, M., Parente, A., Bellemans, A., van Beeck, J., Denys, S., 2021. Application of improved CFD modeling for prediction and mitigation of traffic-related air pollution hotspots in a realistic urban street. *Atmos. Environ.* 246, 118127. <https://doi.org/10.1016/j.atmosenv.2020.118127>.

- Lee, B.E., Soliman, B.F., 1977. An investigation of the forces on three dimensional bluff bodies in lough wall turbulent boundary layers. *Fluids Eng.* 99 (3), 503–509.
- Lin, M., Hang, J., Li, Y., Luo, Z., Sandberg, M., 2014. Quantitative ventilation assessments of idealized urban canopy layers with various urban layouts and the same building packing density. *Build. Environ.* 79, 152–167. <https://doi.org/10.1016/j.buildenv.2014.05.008>.
- Liu, F., Qian, H., Zheng, X., Zhang, L., Liang, W., 2017. Numerical study on the urban ventilation in regulating microclimate and pollutant dispersion in urban street canyon: a case study of Nanjing new region, China. *Atmosphere (Basel)* 8. <https://doi.org/10.3390/atmos8090164>.
- Liu, S., Pan, W., Zhao, X., Zhang, H., Cheng, X., Long, Z., Chen, Q., 2018. Influence of surrounding buildings on wind flow around a building predicted by CFD simulations. *Build. Environ.* 140, 1–10. <https://doi.org/10.1016/j.buildenv.2018.05.011>.
- Llaguno-Muniz, M., Bou-Zeid, E., 2018. Shaping buildings to promote street ventilation: a large-eddy simulation study. *Urban Clim.* 26, 76–94. <https://doi.org/10.1016/j.uclim.2018.08.006>.
- Longo, R., Bellemans, A., Derudi, M., Parente, A., 2020. A multi-fidelity framework for the estimation of the turbulent schmidt number in the simulation of atmospheric dispersion. *Build. Environ.* 185. <https://doi.org/10.1016/j.buildenv.2020.107066>.
- Mei, S.-J., Hu, J.-T., Liu, D., Zhao, F.-Y., Li, Y., Wang, Y., Wang, H.-Q., 2017. Wind driven natural ventilation in the idealized building block arrays with multiple urban morphologies and unique package building density. *Energy Build.* 155, 324–338. <https://doi.org/10.1016/j.enbuid.2017.09.019>.
- Mitchell, D., Kornhuber, K., Huntingford, C., Uhe, P., 2019. The day the 2003 European heatwave record was broken. *Lancet Planet. Heal.* [https://doi.org/10.1016/S2542-5196\(19\)30106-8](https://doi.org/10.1016/S2542-5196(19)30106-8).
- Montazeri, H., Toparlar, Y., Blocken, B., Hensen, J.L.M., 2017. Simulating the cooling effects of water spray systems in urban landscapes: a computational fluid dynamics study in Rotterdam, The Netherlands. *Landsc. Urban Plan.* 159, 85–100. <https://doi.org/10.1016/j.landurbplan.2016.10.001>.
- Monti, P., Leuzzi, G., 2005. A numerical study of mesoscale airflow and dispersion over coastal complex terrain. *Int. J. Environ. Pollut.* 25, 239–250. <https://doi.org/10.1504/ijep.2005.007670>.
- Nardicchia, F., Di Bernardino, A., Pagliaro, F., Monti, P., Leuzzi, G., Gugliemetti, L., 2018. CFD analysis of urban canopy flows employing the V2F model: impact of different aspect ratios and relative heights. *Adv. Meteorol.* <https://doi.org/10.1155/2018/2189234>.
- Neophytou, M.K.-A., Britter, R.E., 2005. Modelling the wind flow in complex urban topographies: a computational-fluid-dynamics simulation of the central London area. *Proceedings of the 5th GRACM International Congress on Comput Mech*, 29 June–1 July, Limassol, 2005, pp. 967–974.
- Ng, E., 2009. Policies and technical guidelines for urban planning of high-density cities - air ventilation assessment (AVA) of Hong Kong. *Build. Environ.* 44, 1478–1488. <https://doi.org/10.1016/j.buildenv.2008.06.013>.
- Nozu, T., Tamura, T., 2012. LES of turbulent wind and gas dispersion in a city. *J. Wind Eng. Ind. Aerodyn.* 104–106, 492–499. <https://doi.org/10.1016/j.jweia.2012.02.024>.
- Oberkampf, W.L., Trucano, T.G., Hirsch, C., 2004. Verification, validation, and predictive capability in computational engineering and physics. *Appl. Mech. Rev.* 57, 345–384. <https://doi.org/10.1115/1.1767847>.
- Oguro, M., Morikawa, Y., Murakami, S., Matsunawa, K., Mochida, A., Hayashi, H., 2008. Development of a wind environment database in Tokyo for a comprehensive assessment system for heat island relaxation measures. *J. Wind Eng. Ind. Aerodyn.* 96, 1591–1602. <https://doi.org/10.1016/j.jweia.2008.02.023>.
- Oke, T.R., 1987. *Boundary Layer Climates*. Second Ed.
- Oke, T.R., 1988. Street design and urban canopy layer climate. *Energy Build.* 11, 103–113. [https://doi.org/10.1016/0378-7788\(88\)90026-6](https://doi.org/10.1016/0378-7788(88)90026-6).
- Oke, T.R., Maxwell, G.B., 1975. Urban heat island dynamics in Montreal and Vancouver. *Atmos. Environ.* 9, 191–200. [https://doi.org/10.1016/0004-6981\(75\)90067-0](https://doi.org/10.1016/0004-6981(75)90067-0).
- Panagiotou, I., Neophytou, M.K.-A., Hamlyn, D., Britter, R.E., 2013. City breathability as quantified by the exchange velocity and its spatial variation in real inhomogeneous urban geometries: an example from Central London urban area. *Sci. Total Environ.* 442, 466–477. <https://doi.org/10.1016/j.scitotenv.2012.09.001>.
- Pelliccioni, A., Monti, P., Leuzzi, G., 2015. An alternative wind profile formulation for urban areas in neutral conditions. *Environ. Fluid Mech.* 15, 135–146. <https://doi.org/10.1007/s10652-014-9364-1>.
- Pelliccioni, A., Monti, P., Cattani, G., Bocconi, F., Cacciani, M., Canepari, S., Capone, P., Catrambone, M., Cusano, M., D'Ovidio, M.C., Santis, A.De, Bernardino, A.Di, Menno, Di, Di Buccianico, A., Renzi, S.Di, Ferrante, R., Gaeta, A., Gaddi, R., Gherardi, M., Giusto, M., Gordiani, A., Grandoni, L., Leone, G., Leuzzi, G., L'Episcopo, N., Marcovecchio, F., Pini, A., Sargolini, T., Tombolini, F., Tofful, L., Perrino, C., 2020. Integrated evaluation of indoor particulate exposure: the VIEPI project. *Sustainability* 12, 9758. <https://doi.org/10.3390/su12229758>.
- Peng, Y., Gao, Z., Buccolieri, R., Ding, W., 2019. An investigation of the quantitative correlation between urban morphology parameters and outdoor ventilation efficiency indices. *Atmosphere (Basel)* 10. <https://doi.org/10.3390/atmos10010033>.
- Peng, Y., Buccolieri, R., Gao, Z., Ding, W., 2020. Indices employed for the assessment of "urban outdoor ventilation" - a review. *Atmos. Environ.* <https://doi.org/10.1016/j.atmosenv.2019.117211>.
- QGIS Documentation, 2021. [https://docs.qgis.org/3.16/en/docs/training\\_manual](https://docs.qgis.org/3.16/en/docs/training_manual).
- Ragioneria Generale I Direzione Sistemi informativi di pianificazione e controllo finanziario U.O. Statistica, 2017. *La popolazione di Roma*.
- Ramponi, R., Blocken, B., de Co, L.B., Janssen, W.D., 2015. CFD simulation of outdoor ventilation of generic urban configurations with different urban densities and equal and unequal street widths. *Build. Environ.* 92, 152–166. <https://doi.org/10.1016/j.buildenv.2015.04.018>.
- Ratti, C., Di Sabatino, S., Britter, R., 2006. Urban texture analysis with image processing techniques: winds and dispersion. *Theor. Appl. Clim.* 84, 77–90. <https://doi.org/10.1007/s00704-005-0146-z>.
- Razak, A.A., Hagishima, A., Ikegaya, N., Tanimoto, J., 2013. Analysis of airflow over building arrays for assessment of urban wind environment. *Build. Environ.* 59, 56–65. <https://doi.org/10.1016/j.buildenv.2012.08.007>.
- Ricci, A., Kalkman, I., Blocken, B., Burlando, M., Freda, A., Repetto, M.P., 2017. Local-scale forcing effects on wind flows in an urban environment: impact of geometrical simplifications. *J. Wind Eng. Ind. Aerodyn.* 170, 238–255. <https://doi.org/10.1016/j.jweia.2017.08.001>.
- Richards, P.J., Hoxey, R.P., 1993. Appropriate boundary conditions for computational wind engineering models using the k-ε turbulence model. *J. Wind Eng. Ind. Aerodyn.* 46–47, 145–153. [https://doi.org/10.1016/0167-6105\(93\)90124-7](https://doi.org/10.1016/0167-6105(93)90124-7).
- Roache, P.J., 1997. Quantification of uncertainty in computational fluid dynamics. *Annu. Rev. Fluid Mech.* 29, 123–160. <https://doi.org/10.1146/annurev.fluid.29.1.123>.
- Salizzoni, P., Marro, M., Soulhac, L., Grosjean, N., Perkins, R.J., 2011. Turbulent transfer between street canyons and the overlying atmospheric boundary layer. *Bound.-Layer Meteorol.* 141, 393–414. <https://doi.org/10.1007/s10546-011-9641-1>.
- Salvadori, L., Badas, M.G., Di Bernardino, A., Querzoli, G., 2021. A street graph-based morphometric characterization of two large urban areas. *Sustainability* 13. <https://doi.org/10.3390/su13031025>.
- Salvati, A., Monti, P., Coch Roura, H., Cecere, C., 2019. Climatic performance of urban textures: analysis tools for a Mediterranean urban context. *Energy Build.* 185, 162–179. <https://doi.org/10.1016/j.enbuid.2018.12.024>.
- Sandberg, M., 1981. What is ventilation efficiency? *Build. Environ.* 16, 123–135. [https://doi.org/10.1016/0360-1323\(81\)90028-7](https://doi.org/10.1016/0360-1323(81)90028-7).
- Santiago, J.L., Coceal, O., Martilli, A., Belcher, S.E., 2008. Variation of the sectional drag coefficient of a Group of Buildings with packing density. *Build. Vent. Theory Meas.* 128, 445–457. <https://doi.org/10.1007/s10546-008-9294-x>.
- Schatzmann, M., Olesen, H., Franke, J., 2010. *Cost 732 Model Evaluation Case Studies: Approach and Results, COST Action*.
- Seaton, A., Godden, D., MacNee, W., Donaldson, K., 1995. Particulate air pollution and acute health effects. *Lancet* 345, 176–178. [https://doi.org/10.1016/S0140-6736\(95\)90173-6](https://doi.org/10.1016/S0140-6736(95)90173-6).
- Sha, C., Wang, X., Lin, Y., Fan, Y., Chen, X., Hang, J., 2018. The impact of urban open space and 'lift-up' building design on building intake fraction and daily pollutant exposure in idealized urban models. *Sci. Total Environ.* 633, 1314–1328. <https://doi.org/10.1016/j.scitotenv.2018.03.194>.
- Shih, T.-H., Liou, W.W., Shabbir, A., Yang, Z., Zhu, J., 1995. A new k-ε eddy viscosity model for high Reynolds number turbulent flows. *Comput. Fluids* 24, 227–238.
- Sini, J.F., Anquetin, S., Mestayer, P.G., 1996. Pollutant dispersion and thermal effects in urban street canyons. *Atmos. Environ.* 30, 2659–2677. [https://doi.org/10.1016/1352-2310\(95\)00321-5](https://doi.org/10.1016/1352-2310(95)00321-5).
- Skote, M., Sandberg, M., Westerberg, U., Claesson, L., Johansson, A.V., 2005. Numerical and experimental studies of wind environment in an urban morphology. *Atmos. Environ.* 39, 6147–6158. <https://doi.org/10.1016/j.atmosenv.2005.06.052>.
- Soulhac, L., Garbero, V., Salizzoni, P., Mejean, P., Perkins, R.J., 2009. Flow and dispersion in street intersections. *Atmos. Environ.* 43, 2981–2996. <https://doi.org/10.1016/j.atmosenv.2009.02.061>.
- Tominaga, Y., 2012. Visualization of city breathability based on CFD technique: case study for urban blocks in Niigata City. *J. Vis.* 15, 269–276. <https://doi.org/10.1007/s12650-012-0128-z>.
- Tominaga, Y., Mochida, A., Yoshie, R., Kataoka, H., Nozu, T., Yoshikawa, M., Shirasawa, T., 2008. AIJ guidelines for practical applications of CFD to pedestrian wind environment around buildings. *J. Wind Eng. Ind. Aerodyn.* 96, 1749–1761. <https://doi.org/10.1016/j.jweia.2008.02.058>.
- Toparlar, Y., Blocken, B., Vos, P., Van Heijst, G.J.F., Janssen, W.D., van Hooff, T., Montazeri, H., Timmermans, H.J.P., 2015. CFD simulation and validation of urban microclimate: a case study for Bergpolder Zuid, Rotterdam. *Build. Environ.* 83, 79–90. <https://doi.org/10.1016/j.buildenv.2014.08.004>.
- Toparlar, Y., Blocken, B., Maiheu, B., van Heijst, G.J.F., 2017. A review on the CFD analysis of urban microclimate. *Renew. Sust. Energ. Rev.* 80, 1613–1640. <https://doi.org/10.1016/j.rser.2017.05.248>.
- Toparlar, Y., Blocken, B., Maiheu, B., van Heijst, G.J.F., 2018. The effect of an urban park on the microclimate in its vicinity: a case study for Antwerp, Belgium. *Int. J. Climatol.* 38, e303–e322. <https://doi.org/10.1002/joc.5371>.
- Tsichritzis, L., Nikolopoulos, M., 2019. The effect of building height and façade area ratio on pedestrian wind comfort of London. *J. Wind Eng. Ind. Aerodyn.* 191, 63–75. <https://doi.org/10.1016/j.jweia.2019.05.021>.
- Tucker, P.G., Mosquera, A., 2001. In: *CFD, N.A.F.E.M.S. (Ed.), NAFEMS Introduction to Grid and Mesh Generation for CFD*.
- Unecce, 2018. Air pollution and health - air pollution - environmental policy [WWW Document]. <https://www.unecce.org/environmental-policy/conventions/envirtpawelcome/cross-sectoral-linkages/air-pollution-and-health.html>.
- United Nations, 2014. *World Urbanization Prospects: The 2014 Revision*, New York, United. <https://doi.org/10.4054/DemRes.2005.12.9>.
- United Nations, 2015. *Transforming our world: the 2030 Agenda for Sustainable Development*. United Nations Sustainable knowledge platform. *Sustain. Dev. Goals* 1–40a.
- United Nations, 2018a. *World Urbanization Prospects: The 2018 Revision*.
- United Nations, 2018b. *The World's Cities in 2018*.
- Urban Atlas 2006, 2014. <https://land.copernicus.eu/local/urban-atlas>.
- van Hooff, T., Blocken, B., 2010. Coupled urban wind flow and indoor natural ventilation modelling on a high-resolution grid: a case study for the Amsterdam ArenA stadium. *Environ. Model. Softw.* 25, 51–65. <https://doi.org/10.1016/j.envsoft.2009.07.008>.
- Vervoort, R., Blocken, B., van Hooff, T., 2019. Reduction of particulate matter concentrations by local removal in a building courtyard: case study for the Delhi american

- embassy school. *Sci. Total Environ.* 686, 657–680. <https://doi.org/10.1016/j.scitotenv.2019.05.154>.
- Watts, N., Amann, M., Arnell, N., Ayeb-Karlsson, S., Belesova, K., Berry, H., Bouley, T., Boykoff, M., Byass, P., Cai, W., Campbell-Lendrum, D., Chambers, J., Daly, M., Dasandi, N., Davies, M., Depoux, A., Dominguez-Salas, P., Drummond, P., Ebi, K.L., Ekins, P., Montoya, L.F., Fischer, H., Georgeson, L., Grace, D., Graham, H., Hamilton, I., Hartinger, S., Hess, J., Kelman, I., Kiesewetter, G., Kjellstrom, T., Kniveton, D., Lemke, B., Liang, L., Lott, M., Lowe, R., Sewe, M.O., Martinez-Urtaza, J., Maslin, M., McAllister, L., Mikhaylov, S.J., Milner, J., Moradi-Lakeh, M., Morrissey, K., Murray, K., Nilsson, M., Neville, T., Oreszczyn, T., Owfi, F., Pearman, O., Pencheon, D., Pye, S., Rabbaniha, M., Robinson, E., Rocklöv, J., Saxer, O., Schütte, S., Semenza, J.C., Shumake-Guillemot, J., Steinbach, R., Tabatabaei, M., Tomei, J., Trinanes, J., Wheeler, N., Wilkinson, P., Gong, P., Montgomery, H., Costello, A., 2018. The 2018 report of the lancet countdown on health and climate change: shaping the health of nations for centuries to come. *Lancet* 392, 2479–2514. [https://doi.org/10.1016/S0140-6736\(18\)32594-7](https://doi.org/10.1016/S0140-6736(18)32594-7).
- Wen, C.Y., Juan, Y.H., Yang, A.S., 2017. Enhancement of city breathability with half open spaces in ideal urban street canyons. *Build. Environ.* 112, 322–336. <https://doi.org/10.1016/j.buildenv.2016.11.048>.
- WHO, 2016. WHO Expert Consultation: Available Evidence for the Future Update of the WHO Global Air Quality Guidelines (AQGs). Meeting Report. Bonn, Germany, 29 September– 1 October 2015.
- Wieringa, J., 1992. Updating the Davenport roughness classification. *J. Wind Eng. Ind. Aerodyn.* 41, 357–368. [https://doi.org/10.1016/0167-6105\(92\)90434-C](https://doi.org/10.1016/0167-6105(92)90434-C).
- Xiaomin, X., Zhen, H., Jiasong, W., 2006. The impact of urban street layout on local atmospheric environment. *Build. Environ.* 41, 1352–1363. <https://doi.org/10.1016/j.buildenv.2005.05.028>.
- Xie, X., Huang, Z., Wang, J., Xie, Z., 2005a. The impact of solar radiation and street layout on pollutant dispersion in street canyon. *Build. Environ.* 40, 201–212. <https://doi.org/10.1016/j.buildenv.2004.07.013>.
- Xie, X., Huang, Z., Wang, J.S., 2005b. Impact of building configuration on air quality in street canyon. *Atmos. Environ.* 39, 4519–4530. <https://doi.org/10.1016/j.atmosenv.2005.03.043>.
- Yakhot, V., Orszag, S.A., 1986. Renormalization group analysis of turbulence. I. Basic theory. *J. Sci. Comput.* 1, 3–51. <https://doi.org/10.1007/BF01061452>.
- Yang, F., Qian, F., Lau, S.S.Y., 2013. Urban form and density as indicators for summertime outdoor ventilation potential: a case study on high-rise housing in Shanghai. *Build. Environ.* 70, 122–137. <https://doi.org/10.1016/j.buildenv.2013.08.019>.
- Yim, S.H.L., Fung, J.C.H., Lau, A.K.H., Kot, S.C., 2009. Air ventilation impacts of the “wall effect” resulting from the alignment of high-rise buildings. *Atmos. Environ.* 43, 4982–4994. <https://doi.org/10.1016/j.atmosenv.2009.07.002>.
- Yoshie, R., Mochida, A., Tominaga, Y., Kataoka, H., Harimoto, K., Nozu, T., Shirasawa, T., 2007. Cooperative project for CFD prediction of pedestrian wind environment in the architectural Institute of Japan. *J. Wind Eng. Ind. Aerodyn.* 95, 1551–1578. <https://doi.org/10.1016/j.jweia.2007.02.023>.